226 Corneal imaging and topography
Monday, May 04, 2015 8:30 AM–10:15 AM
Exhibit Hall Poster Session
Program #/Board # Range: 1608–1645/D0116–D0153
Organizing Section: Cornea
Contributing Section(s): Multidisciplinary Ophthalmic Imaging

Program Number: 1608 **Poster Board Number:** D0116
Presentation Time: 8:30 AM–10:15 AM
Anterior Segment Evaluation in healthy Brazilian children with Scheimpflug topography
Matheus Ivan Schmitz Vieira, Arnaldo Maluf Germano Filho, Camila Zangalli, Rosane S. Castro, Andre Okanobo. Ophthalmology, Universidade Estadual de Campinas - UNICAMP, Campinas, Brazil.
Purpose: To identify the distribution and variation of corneal topography, thickness, and elevation measured by the Pentacam (Oculus Optikgeräte GmbH, Wetzlar, Germany) Scheimpflug system in healthy Brazilian children.
Methods: Healthy children aged between 7 and 11 years were scanned with the Pentacam Scheimpflug corneal topography system (Oculus Optikgeräte GmbH, Wetzlar, Germany). The exclusion criteria was the Modified Rabinowitz/McDonnell criteria for keratoconus. Right eye of each subject was selected for analysis. The following parameters were evaluated: central corneal thickness (CCT), thinnest pachymetry (TP), average pachymetric progression index (PPI ave), anterior and posterior elevation thinnest point (AETP and PETP), anterior and posterior best-fit sphere (ABFS and PBFS), pachymetric difference between the apex and the thinnest point (PDAT), ART MAX, Belin/Ambrósio Enhanced Ectasia Display overall index (D), Sim K, Sim K astigmatism, K max and Q value.
Results: A total of 160 children (69 boys, 91 girls) were included in this study. Table 1 summarizes our findings. The mean age of the children was 8.82 ± 1.23 years (range, 7 to 11 y). The mean CCT was 553.81 ± 32 μm and mean TP was 547.95 ± 32.06 μm. The TP was most commonly located in the inferotemporal quadrant compared to the corneal apex in 93,125% (149) eyes. The PPI ave mean was 1.00 ± 0.14 comparable to normal adults (Ambrósio et al, J Refract Surg. 2011;27(10):753-758; Vázquez, Am J Ophthalmol. 2014;158:32–40). The mean of ABFS and PBFS was 7.49 ± 3.26 and 10.54 ± 6.25. ART MAX and D had an average of 446.57 ± 81.20 and 0.78 ± 0.65. Mean ± SD values for Sim K, Sim K astig and K max was 43.35 ± 1.31 D, 0.92 ± 0.66 D and 44.40 ± 1.45 D respectively. The indices in K max and Sim K astig were close to what was reported in other topographic systems in children (Reddy, J Pediatr Ophthalmol Strabismus. 2013;50(5):304-310).
Conclusions: This study provides Pentacam normative values for corneal topography, thickness and elevation in healthy Brazilian children. These results may provide helpful information for diagnosis of corneal diseases in children. Further studies are needed to evaluate the role of tomography in identifying early forms of ectasia in children.

Table 1. Outcome Measures of 160 Children's Eyes Evaluated Using Oculus Pentacam Scheimpflug Topography System

	Mean ± SD	Range	95% CI	Skew	Kurtosis
Age (y)	8.82 ± 1.23	7 to 11	8.626226 to 9.011274	-0.06	-1.13
CCT (μm)	553.81 ± 32	481 to 640	548.8156 to 558.8094	0.06	-0.67
TP (μm)	547.95 ± 32.06	469 to 629	542.9435 to 552.9565	0.05	-0.64
PPI ave	1.00 ± 0.14	0.64 to 1.45	0.9740698 to 1.0164302	0.31	0.29
AETP (μm)	3.20 ± 1.91	1 to 13	2.901379 to 3.498621	1.15	4.88
PETP (μm)	5.09 ± 3.43	2 to 20	4.551641 to 5.623359	0.92	2.20
ABFS	7.49 ± 3.26	4 to 26	6.977863 to 7.997137	1.05	6.33
PBFS	10.54 ± 6.25	3 to 30	9.571570 to 11.21842	0.44	0.26
PDAT (μm)	5.86 ± 4.90	0 to 32	5.097089 to 6.627911	2.69	8.84
ART MAX	446.57 ± 81.20	223 to 745	433.8967 to 459.2533	0.54	0.83
D	0.78 ± 0.65	1.14 to 2.42	0.6793938 to 0.8829812	0.13	0.15
Sim K	43.35 ± 1.31	39.65 to 47.00	43.15 to 43.55	0.058	0.112
Sim K flat	42.95 ± 1.32	39.10 to 46.70	42.73962 to 43.15200	0.04	-0.23
Sim K steer	43.86 ± 1.40	40.20 to 48.00	43.64318 to 44.08182	0.21	-0.07
Sim K Astig	0.92 ± 0.66	4.80 to 0	0,81773 to 1,02227	-1.70	10.95
K Max	44.40 ± 1.45	40.50 to 48.50	44.17616 to 44.62759	0.15	-0.02
Q Value	0,38 ± 0.15	0.77 to 0.56	-0.4015258 to -0.3550992	1.88	10.57

SD = Standard deviation; 95% CI = Confidence interval; CCT = central corneal thickness;
TP = thinnest pachymetry; PPI ave = average pachymetric progression index;
AETP = anterior elevation thinnest point; PETP = posterior elevation thinnest point;
K = keratometry; Sim K = simulated keratometry; ABFS = anterior best fit sphere;
PBFS = posterior best fit sphere; PDAT = pachymetric difference between the apex and the thinnest point; K Max = maximum keratometry; D = Belin/Ambrósio Enhanced Ectasia Display overall index

Table 1. Outcome Measures of 160 Children's Eyes Evaluated Using Oculus Pentacam Scheimpflug Topography System

Commercial Relationships: Matheus Ivan Schmitz Vieira, None; **Arnaldo Maluf Germano Filho**, None; **Camila Zangalli**, None; **Rosane S. Castro**, None; **Andre Okanobo**, None

Program Number: 1609 **Poster Board Number:** D0117
Presentation Time: 8:30 AM–10:15 AM
Topographic screening for corneal abnormalities in a young Jewish population
Emilia Cantera, Magdalena Cortes, Renèe Dattilo. Ospedale Israelitico, Roma, Italy.
Purpose: To screen a population of Jewish children and teenagers living in Rome (Italy) for corneal abnormalities in particular for keratoconus.
Methods: 542 eyes of 271 students, ages 10 to 20 have been examined at the Hebrew School of Rome, using Sirius corneal topographer (CSO), a combination between a rotating Scheimpflug camera and a Placido disk. Minimum corneal thickness, central corneal thickness, 5 mm cylinder front and total, anterior and posterior corneal asymmetry and other useful corneal indices have been evaluated.
Results: A total of 127 boys and 144 girls participated in the study. Corneal topography suggestive strongly for corneal abnormality was present in both eyes of 1 student (0,36%). Corneas examined showed a prolate profile. Anterior Mean simK avg was 7,751 (SD 0,81); minimum corneal thickness was 547,99 (SD30,55), central corneal thickness was 551,46 (SD 30,56) mean 5 mm cylinder front was -0,79 (SD 0,44) and total was 0,55 (SD 0,36), anterior corneal asymmetry was -0,058 (SD 0,53) and posterior corneal asymmetry was 0,0041 (SD 0,93).
Conclusions: corneas examined had a normal prolate profile. Although the studied population belongs to a closed community and previous studies report one of the most elevated world prevalences of keratoconus in Jewish population (2%), the prevalence of corneal abnormalities in our study was not the same. Many explanations should be given. The prevalence of abnormal corneas was 0,36%, probably had an early keratoconus.
Commercial Relationships: Emilia Cantera, None; **Magdalena Cortes**, None; **Renèe Dattilo**, None

Program Number: 1610 **Poster Board Number:** D0118
Presentation Time: 8:30 AM–10:15 AM
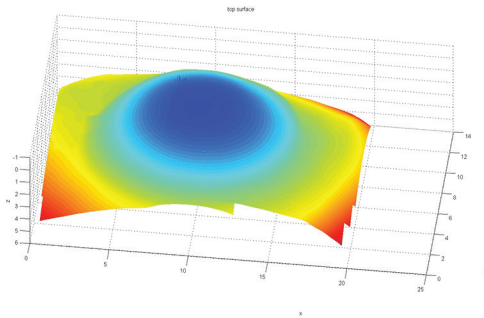**OCT-based eye topographer**
Mircea Mujat, Ankit Patel, Patrick O'Grady, Gopi Maguluri, Nicusor Iftimia, R D. Ferguson. Physical Sciences, Inc., Andover, MA.
Purpose: To develop a novel technology that will allow for precise real-time wide-area measurement of the human eye anterior segment topography. An automated method to measure the complete corneal and scleral topology will provide a valuable tool for both clinicians and scleral lens manufacturers and will help streamline the fitting process.
Methods: An Optical Coherence Tomography (OCT) – based topographer has been developed for rapid measurement of the corneal and scleral topography with micron scale resolution. Radial scanning geometry has been chosen for the OCT imager, in which a pair of elliptical mirrors is used to relay the pivot point from the scanners into the center of the eye, such that the laser beam is always near-normal to the eye surface as the beam scans over the eye surface. Several individual patches (9 mm x 16 mm) are acquired from different locations on the cornea/sclera and are stitched together to generate a large area (20 – 24 mm diameter) eye surface topography. The eye position is controlled by a set of LED fixation lights that turn on sequentially. A USB camera monitors the eye position for easy alignment and during the OCT scan for motion artifacts. Custom software automatically segments the OCT data for surface identification and stitches multiple surfaces together.
Results: The imager was tested on phantoms, a calibration sphere, and animal eyeballs. Were found the smoothness and accuracy of the investigated surfaces to be within the instrument lateral and axial resolution range, which falls within the natural shape deformation and tear film variations in the human eye. The mean error between the surface of the calibration sphere and the OCT measured surface was about 10 μm. Figure 1 shows the large-area surface of a porcine eye obtained by stitching together 10 individual patches.
Conclusions: We have developed an automated corneal/scleral surface topographer with which patients with corneal diseases and disorders can be fitted with scleral hard contact lenses providing comfort, care, and increased treatment options for this patient population. Although preliminary, our results demonstrate the capability of our proposed approach for generating accurate surface plots over relatively large areas of the eye, which is not currently possible with any other single, existing platform.

Contour plot of a porcine eye. Axes are in mm.
Commercial Relationships: Mircea Mujat, Physical Sciences Inc. (P); **Ankit Patel**, None; **Patrick O'Grady**, None; **Gopi Maguluri**, None; **Nicusor Iftimia**, None; **R D. Ferguson**, Physical Sciences Inc. (P)
Support: DOD grant W81XWH-12-C-0116

Program Number: 1611 **Poster Board Number:** D0119
Presentation Time: 8:30 AM–10:15 AM
Simultaneous Retinal and Anterior Segment OCT Imaging with Tunable Lens Technology
Ireneusz Grulkowski, Karol Karnowski, Maciej Wojtkowski. Institute of Physics, Nicolaus Copernicus University, Torun, Poland.
Purpose: To demonstrate the performance of OCT system utilizing tunable lens technology for *in vivo* high-speed simultaneous anterior segment and retinal imaging of the eye. To develop simple interface capable of dynamic control of the optical beam focus.
Methods: A high speed high resolution Fourier-domain OCT instrument operating at 840 nm was developed. An interface of the system was equipped with electrically tunable lens that enabled consecutive focusing of the light beam on anterior segment or the retina. This novel approach allowed for coupling both imaging modes in a simple system without removal of any optical components. OCT imaging was performed on five eyes (5 subjects, mean age 26.2±2.8). Later on, the OCT volumetric data sets were corrected for light refraction distortions to generate images with true shapes of ocular structures.
Results: We characterized the system to optimize its performance parameters. We obtained volumetric OCT tomograms of the anterior segment of the eye and the retina for 3-D visualization of the eye at an imaging speed up to 100,000 axial scans per second and with total imaging depth of 2x5 mm. Comprehensive large scale volumetric data sets (100x250x2048 voxels) containing both anterior segment and retinal structures enabled true reconstruction of the ocular shape. The data provided also access to quantitative description of the eye.
Conclusions: Application of tunable lens technology and its integration with OCT instrument enable automatic compensation of the ocular optics and provide ability to image both parts of the eye simultaneously. This approach enhances functionality of OCT devices and can simplify examination schemes.
Commercial Relationships: Ireneusz Grulkowski, None; **Karol Karnowski**, None; **Maciej Wojtkowski**, None
Support: Polish Ministry of Science and Higher Education (IUVENTUS), Polish National Science Center (#2011/02/A/ST2/00302), Foundation for Polish Science (TEAM/2011-8/8)

Program Number: 1612 **Poster Board Number:** D0120
Presentation Time: 8:30 AM–10:15 AM
AGREEMENT OF CENTRAL CORNEAL THICKNESS with the CASIA SS-1000 ASOCT and ULTRASOUND PACHYMETRY
Eric L. Crowell[1, 2], Alice Chuang[1], Lauren Blieden[1, 2]. [1]Ruiz Department of Ophthalmology and Visual Science, The University of Texas Medical School at Houston, Houston, TX; [2]Robert Cizik Eye Clinic, Houston, TX.
Purpose: Using a retrospective review, determine the agreement of central corneal thickness (CCT) measurements taken by the CASIA SS-1000 Anterior Segment Ocular Coherence Tomography (ASOCT; Tomey, Nagoya, Japan) with those taken by ultrasound pachymetry (USP), the current clinical gold-standard.
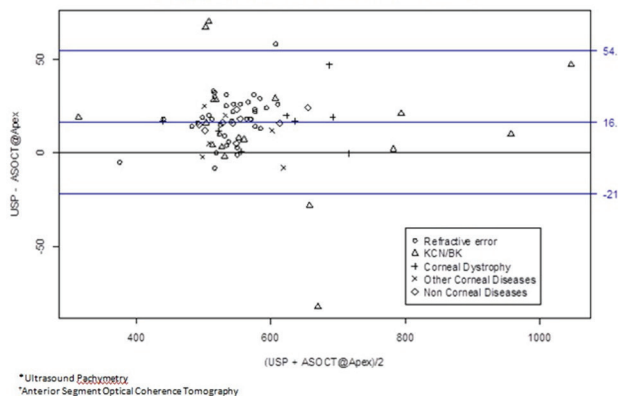**Methods:** Patients who had undergone ASOCT imaging using the 'Corneal Map Mode were reviewed. Participants were included if they had CCT measured by USP on the same date as ASOCT imaging. Patients were excluded if they had anterior segment abnormalities or media opacities that affected the cornea or measurements. If both eyes were eligible, one eye was randomly selected. Eyes were classified into 5 groups: refractive error, keratoconus (KCN)/bullous keratopathy (BK), corneal dystrophy, other corneal diseases, and non-corneal ocular diseases. Agreement

was evaluated by the mean difference between ASOCT and USP and limits of agreement.

Results: Seventy-eight eyes from 78 participants were included. The mean age of participants was 41.0 (± 19.0) years with 42 (53.8%) male, 32 (42.7%) white, and 34 (43.6%) right eyes. Mean IOP was15.0 (± 5.5) mm Hg. Thirty-seven (47.4%) eyes had refractive error, 18 (23.1%) KCN/BK, 8 (10.3%) corneal dystrophy, 6 (7.7%) other corneal disease, and 9 (11.5%) noncorneal ocular diseases. Previous surgeries included 5 (6.4%) partial thickness penetrating keratoplasty, 5 (6.4%) full thickness penetrating keratoplasty, 5 (5.1%) LASIK, 2 (2.6%) photorefractive keratectomy, and 2 (2.6%) filtration surgery. Sixty-five (82.3%) eyes were phakic, 13 (16.5%) pseudophakic, and one (1.3%) aphakic. On average the CASIA SS-1000 ASOCT underestimates CCT by -16μm (Figure 1). The magnitude of agreement between the 2 instruments did not vary according to corneal thickness The limits of agreement show a 95% variation within 38μm, with 5 eyes outside the limits of agreement. Four of these 5 consist of those eyes with KCN/BK, and one eye with myopia & regular astigmatism.

Conclusions: The CASIA SS-1000 is similar to other ASOCT machines in that it gives a CCT reading lower than the USP, the current gold standard. KCN eyes tend to have larger differences in CCT measurement between ASOCT and USP. This difference may indicate that one modality of CCT measurement is more appropriate in KCN eyes.

Figure 1. Bland-Altman Plot USP* - ASOCT†

*Ultrasound Pachymetry
†Anterior Segment Optical Coherence Tomography

Brand-Altman between USP and ASOCT

Commercial Relationships: Eric L. Crowell, None; **Alice Chuang**, None; **Lauren Blieden**, None

Comparison of Ultrasound and OCT Corneal and Epithelial Thickness Maps
Raksha Urs[1], Harriet O. Lloyd[1], Ronald H. Silverman[1, 2].
[1]Ophthalmology, Columbia University Medical Center, Teaneck, NJ;
[2]Riverside Research, New York, NY.
Purpose: The goal of this study was to compare measurements of corneal and epithelial thickness maps obtained by the RTVue OCT system with those obtained from the Artemis immersion scanning high-frequency ultrasound system and to assess the agreement between the two devices.

Methods: Both eyes of 10 normal volunteers were scanned with the Artemis and RTVue. For each corneal thickness map, the minimum corneal thickness (MCT) and mean corneal thickness in 0.5 mm-wide annuli of up to 3 mm radius around the location of MCT were determined. From the epithelial maps, the value of epithelial thickness (ET) at the location of the MCT and mean epithelial thickness in 0.5mm-wide annuli around the location of MCT was determined.

Results: Thickness measurements from Artemis and RTVue thickness maps were 514.3 ± 35.2 μm and 513.6 ± 33.6 μm respectively for MCT and 55.1 ± 2.8 μm and 53.8 ± 3.4 μm for ET. There was high correlation between both the MCT and ETreadings by the two methods (R = 0.99 for MCT and R = 0.78 for ET). Bland-Altman analysis showed that there was no difference between MCT values obtained from the two methods. The mean ET values obtained from Artemis exceeded RTVue values by 1.2 μm. Mean corneal thickness values and epithelial thickness values in each of the 0.5 mm annuli were also highly correlated (R>0.92 for corneal thickness values and R>0.74 for epithelial thickness values). Mean Artemis epithelial thickness values in 0.5 mm annuli rings were slightly higher than RTVue values (1.6 – 2.17 μm). T-testrevealed that the difference in measurements from the two devices were statistically significant. Qualitative inspection of epithelial maps from the two devices revealed similar appearance, but with features appea

Conclusions: Artemis and RTVue corneal and epithelial thickness measurements in the 3 mm radius zone are highly correlated in normal eyes. Artemis epithelial maps were systemically thicker than RTVue epithelial maps. We surmise that this difference could be attributed to signal processing and determination of the back surface of the epithelium.

Commercial Relationships: Raksha Urs, None; **Harriet O. Lloyd**, None; **Ronald H. Silverman**, Arcscan Inc (S), Cornell Research Foundation (P)

Confocal Microscopy for Diagnosis of Acanthamoeba Keratitis: Nidek versus Heidelberg
Jeffrey R. Golen, Jeremy D. Keenan. F.I. Proctor Foundation, University of California, San Francisco, San Francisco, CA.
Purpose: To compare the diagnostic utility of the Nidek and Heidelberg systems for acanthamoeba keratitis.

Methods: The Nidek Confoscan4 and the Heidelberg HRT3 Rostock confocal microscopes were used in a consecutive series of patients suspected of having acanthamoeba keratitis. Images from both microscopes were presented in a random order to two masked graders. Examiners graded each series of images for the presence or absence of acanthamoeba cysts, and also documented whether their evaluation was made with a low or high degree of certainty. Graders discussed discrepancies and agreed on a single grade and level of certainty for all scans.

Results: 18 total scans from 13 eyes were evaluated, including 5 eyes that were smear- or culture-positive and had examinations performed on both microscopes, and 8 control eyes that were smear-and/or and culture-negative, but exhibited suspicious keratitis clinically. Five control eyes were tested on the Nidek only and 3 control eyes were tested on the Heidelberg only. For the Heidelberg camera, all 5 smear- or culture-positive cases were correctly interpreted by expert examiners (sensitivity=100%, 95%CI 47.8 to 100%), and all 3 negative cases were correctly interpreted as negative (specificity=100%, 95%CI 29.2 to 100%). For the Nidek, 3 of 5

smear- or culture-positive cases were correctly identified by expert examiners as positive (sensitivity 60%, 95%CI 14.7 to 94.7%), and 5 out of 5 negative cases were correctly interpreted as negative (specificity=100%, 95%CI 47.8 to 100%). Of the five positive cases for each camera, 2 cases were identified as "high certainty" on each machine. There was no difference between the two microscopes among the 5 eyes that had both scans performed (P=0.50, McNemar's test).

Conclusions: Both the Nidek and Heidelberg confocal microscopes are useful in diagnosis of acanthamoeba keratitis. Although not statistically significant in this small study, the Heidelberg microscope appeared to be more effective in identifying acanthamoeba cysts than the Nidek. Neither microscope produced false positive tests. These results could be dependent on the graders from this specific study and should be confirmed in future studies.
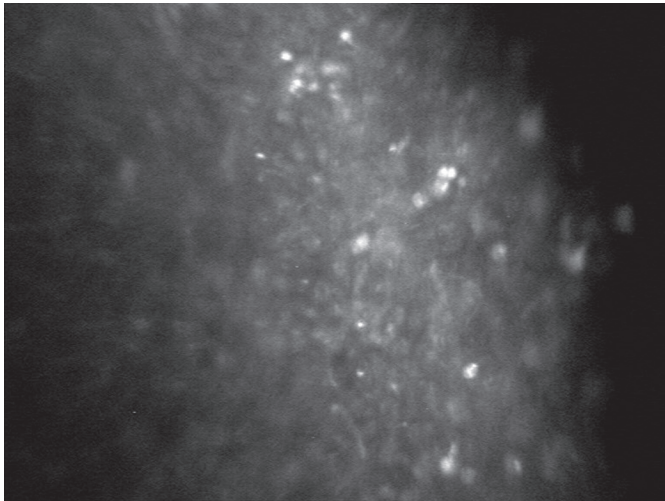

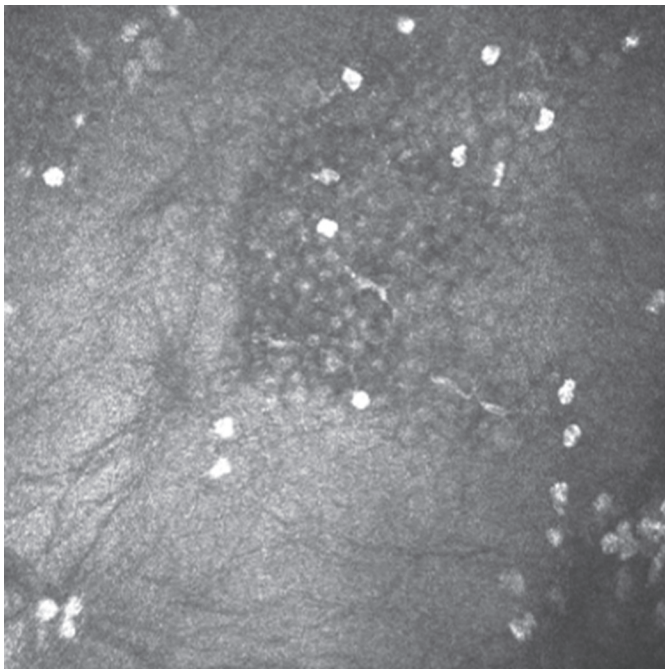Figure 1a: Acanthamoeba cysts seen on Nidek Confoscan4

Figure 1b: The same eye, showing acanthamoeba cysts seen with the Heidelberg HRT3 Rostock confocal microscope

Commercial Relationships: Jeffrey R. Golen, None; **Jeremy D. Keenan**, None

Program Number: 1615 **Poster Board Number:** D0123
Presentation Time: 8:30 AM–10:15 AM
Optical Coherence Tomography findings in Recurrent Corneal Erosion Syndrome
Juan A. Duran, Elío Díez-Feijóo. Instituto de Oftalmologia, Basque Country University, Vizcaya, Spain.
Purpose: To report the findings from the Optical Coherence Tomography (OCT) in the cornea of patients with Recurrent Corneal Erosion Syndrome (RCES).
Methods: 10 normal subjects and 25 RCES patients were recruited for the study. 10 RCES patients, suffered from an acute episode of pain and 15 patients complained of the typical chronic symptoms of RCES. All eyes were scanned with the Anterior segment 5 line raster acquisition protocol of the Cirrus HD-OCT platform (Zeiss, Germany). The etiology of RCES was investigated and treatment was applied following a standard clinical protocol. Scans were obtained at different stages of the pathology and we performed follow-up of each patient following treatment.
Results: Tear film, epithelium, basement membrane, Bowman layer, stroma and Descemet's-endothelium complex were identified by OCT in all normal corneas. Same structures were identified in non-affected areas of RCES corneas. Patients suffering from acute RCES showed the following OCT findings: anterior stromal hyper-refletivity (100%), epithelial edema (100%) and irregular breaks in the epithelium (90%). Patients with chronic RCES presented areas with undetected epithelial basement membrane (100%), intraepithelial basement membrane (60%), intraepithelial inclusions (60%) and anterior stromal hyper-reflectivity (40%). These findings correlated well with the clinical symptoms and with the previously described histological reports of RCES.
Conclusions: Corneal OCT can be useful to study and manage RCES. Specific OCT findings may clarify etiology, confirm a suspected diagnosis and give advice on the decision to treat patients.
Commercial Relationships: Juan A. Duran, None; **Elío Díez-Feijóo**, None

Program Number: 1616 **Poster Board Number:** D0124
Presentation Time: 8:30 AM–10:15 AM
Measurement of Corneal Backscatter by Scheimpflug and Confocal Microscopy
Jay W. McLaren, Katrina M. Kane, Katrin Wacker, Sanjay V. Patel. Ophthalmology, Mayo Clinic, Rochester, MN.
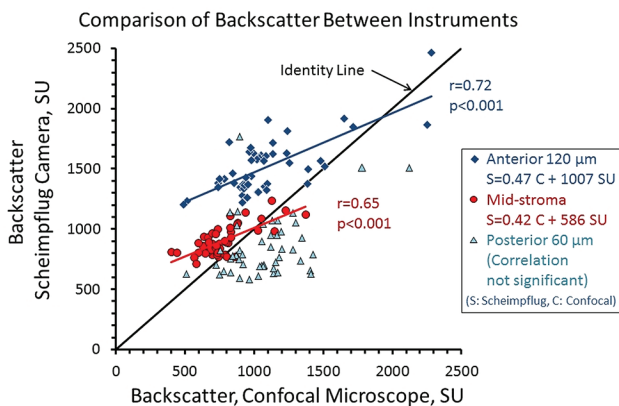**Purpose:** The Scheimpflug camera can provide fast, non-contact estimates of corneal haze (backscatter) from image brightness, but it is unknown if these estimates are equivalent to measurements of corneal haze from other instruments. In this study we compared backscatter estimated from a Scheimpflug camera with backscatter estimated from a clinical confocal microscope in a group of subjects with a wide range of corneal haze.
Methods: Forty eyes from 25 patients with Fuchs Endothelial Dystrophy (high haze) and 12 eyes from 6 normal participants (low haze) were examined by using a Scheimpflug camera (Pentacam, Oculus). The mean image brightness (backscatter) from the anterior 120 μm, mid-stroma, and posterior 60 μm of the cornea, across the central 2 mm were calculated by the native software. The same eyes were then scanned by using a clinical confocal microscope (ConfoScan 4, Nidek Technologies) and mean image brightness at similar anterior, mid-stromal, and posterior depths was calculated. Image brightness from each instrument was standardized to a

fixed scatter source and expressed as "Scatter Units" (SU), the concentration of Amco Clear (GFS Chemicals) that gave the same image brightness as the corneal image. Generalized estimating equation models (paired tests and regression) were used to explore differences and correlation between the two instruments and to adjust for possible correlation between fellow eyes of the same subject.
Results: Backscatter measured by the Scheimpflug camera in the anterior and mid-stroma were correlated with backscatter measured by the confocal microscope (p<0.001), although the mean slope of the regression lines was 0.45 (Figure). Mean backscatter from the anterior and mid-stroma were greater with the Scheimpflug camera than with the confocal microscope (p<0.001). Backscatter from the posterior cornea was lower when measured by the Scheimpflug camera (p<0.001).
Conclusions: The relationship between backscatter measured by these two instruments varies with depth in the cornea. Differences may be from the optical design of each instrument and the ratio of scattered to reflected light. These instruments should not be used interchangeably for measuring corneal haze.

Comparison of Backscatter Between Instruments

Commercial Relationships: Jay W. McLaren, None; **Katrina M. Kane**, None; **Katrin Wacker**, None; **Sanjay V. Patel**, None
Support: Research to Prevent Blindness, Mayo Foundation

Program Number: 1617 **Poster Board Number:** D0125
Presentation Time: 8:30 AM–10:15 AM
Assessment of Contralateral Eye in Unilateral Keratoconus using Artemis Epithelial Maps
Ronald H. Silverman[1], Raksha Urs[1], Timothy J. Archer[2], Marine Gobbe[2], Dan Z. Reinstein[2, 1]. [1]Ophthalmology, Columbia University Medical Center, New York, NY; [2]London Vision Clinic, London, United Kingdom.
Purpose: Although keratoconus (KC) is regarded as a bilateral disease, in some instances, patients initially present unilaterally, with the fellow eye appearing normal clinically and topographically. Such eyes are considered to represent the gold standard for evaluation of methods for early KC detection. In this study we assessed the effectiveness of a KC detection algorithm derived from Artemis very high frequency ultrasound epithelial thickness maps in 12 unilateral KC subjects.
Methods: Subjects were recruited from a population of candidates for corneal refractive surgery presenting at the London Vision Clinic. The study included clinically and topographically normal fellow eyes of 12 patients with unilateral moderate to advanced KC. We acquired Artemis scan data and applied a previously developed linear

discriminant analysis multivariate model for separation of normal and advanced KC based on Artemis epithelial thickness maps to the asymptomatic fellow eyes. Pentacam Belin-Ambrosio Display (BAD) data were available for 7 of the 12 eyes.
Results: Four of the 12 fellow eyes were classified as KC by the Artemis model. Three cases classified as normal by the algorithm, however, exhibited an epithelial pattern suggestive of KC to an expert observer. Of the 7 fellow eyes with both Pentacam and Artemis data, only one was classified as KC by the Artemis algorithm, a different eye by Pentacam (BAD-D >1.5) and yet another by a combined Artemis plus Pentacam model. Three of the 7 fellow eyes with Pentacam data were classified as normal by all three methods (BAD-D values of -0.39, +0.07, +0.5).
Conclusions: We know that in a significant proportion of cases, epithelial remodeling manifests prior to changes in topography and masks early KC topographically. Assuming that KC is a bilateral disease and that its expression may be asymmetric, we have demonstrated that one third of 'normal' fellow eyes could be found to have KC by using epithelial thickness maps. The combination of topographic BAD criteria with epithelial maps did not appear to perform better. Possibly this population included patients who were truly monocularly keratoconic. Alternatively, it may be that the phenotypically unexpressed form of KC might actually be undetectable by anatomical analysis: this would explain the rare cases of post-LASIK ectasia "without a cause". Perhaps in vivo localized biomechanical evaluation may be required to detect such cases.
Commercial Relationships: Ronald H. Silverman, Arcscan, Inc. (I); **Raksha Urs**, None; **Timothy J. Archer**, None; **Marine Gobbe**, None; **Dan Z. Reinstein**, Arcscan, Inc. (I)
Support: NIH Grants EY019055, P30 EY019007 and Research to Prevent Blindness

Program Number: 1618 **Poster Board Number:** D0126
Presentation Time: 8:30 AM–10:15 AM
A new Zernike algorithm to link asymmetric corneal thickness to corneal wavefront aberrations for diagnosis of keratoconus
Purnima R Srivatsa[1], Rohit Shetty[1, 2], Himanshu Matalia[1], Abhijit Sinha Roy[1]. [1]Narayana Nethralaya, Bangalore, India, Bangalore, India; [2]Singapore Eye Research Institute, Singapore, Singapore.
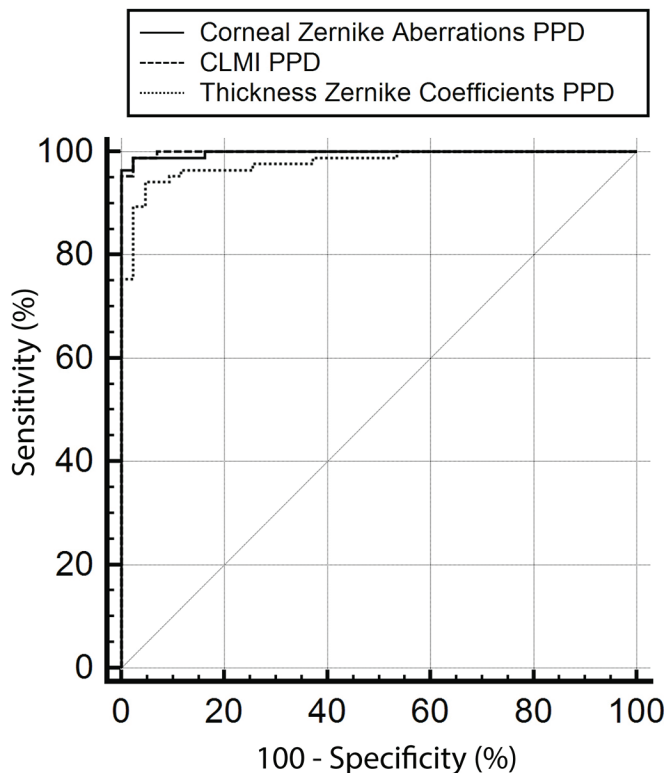**Purpose:** To correlate Zernike interpolation of spatial corneal thickness with corneal wavefront aberrations and assess its diagnostic sensitivity and specificity
Methods: Corneal tomography of 44 normal and 92 keratoconus (KC) corneas was assessed with Pentacam (OCULUS Optikgerate Gmbh, Germany). Using mean keratometry, a custom severity scale was used to grade KC corneas from 1 to 3. Zernike analysis of anterior surface aberrations was performed using ray tracing. A novel Zernike formulation was used to map the spatially varying thickness of the corneas. Both aberrations and thickness mapping with Zernike yielded familiar coefficients, e.g., defocus, coma. The 2nd, 3rd and higher order root mean square (RMS) of the Zernike coefficients from both aberrations and thickness mapping were analyzed with stepwise logistic regression. Also, cone location magnitude index of the anterior and posterior surface using both axial (aCLMI) and tangential curvature (tCLMI) were analyzed with logistic regression. Area under the receiver operating characteristics curve (AUROC) of each regression was compared along with their corresponding sensitivity (Se) and specificity (Sp). A p-value<0.05 was considered to be statistically significant.
Results: Among aberrations variables, 2nd and 3rd order Zernike RMS of aberrations were the best indicators of KC (p<0.0001, AUROC=0.998, Se=98.8%, Sp=97.7%). Among thickness variables, minimum corneal thickness, 2nd and 3rd order Zernike

RMS of thickness map were the best indicators of KC (p<0.0001, AUROC=0.978, Se=94.2%, Sp=95.4%). Among CLMI variables, aCLMI of posterior and tCLMI of anterior surface were the best indicators of KC (p<0.0001, AUROC=0.965, Se=98.8%, Sp=97.7%). Comparison of the ROC curves of the three regression models did not yield any statistically significant difference between them (CLMI vs. corneal Zernike aberrations: p=0.77; CLMI vs. thickness Zernike: p =0.06; Corneal Zernike aberrations vs. thickness Zernike: p=0.06). ROC curves are shown in figure. There was significant linear correlation between RMS of corneal aberration and thickness Zernike coefficients (minimum r = 0.69, p<0.0001).
Conclusions: A new Zernike method of mapping corneal thickness in KC was developed. The Zernike mapping of thickness had diagnostic efficacy similar to using Zernike mapping of corneal wavefront aberrations and CLMI indices.

ROC curves of study indices
Commercial Relationships: Purnima R Srivatsa, None; **Rohit Shetty**, None; **Himanshu Matalia**, None; **Abhijit Sinha Roy**, Avedro (C), Carl Zeiss (C), Cleveland Clinic Cole Eye Institute (P), Topcon (C)

Program Number: 1619 Poster Board Number: D0127
Presentation Time: 8:30 AM–10:15 AM
Diagnostic value of entire vertical thickness profiles of epithelium and Bowman's layer for sub-clinical keratoconus using ultra-high resolution optical coherence tomography
Meixiao Shen[1], Zhe Xu[1], Mei Peng[1], Jun Jiang[1], Jianhua Wang[2], Fan Lv[1]. [1]Wenzhou Medical University, Wenzhou, China; [2]Bascom Palmer Eye Institute, Miami, FL.
Purpose: To evaluate the diagnostic value of vertical thickness profiles of epithelium and Bowman's layer for sub-clinical keratoconus (KC) using ultra-high resolution optical coherence tomography (UHR-OCT).

Methods: Eighty-one eyes of 81 normal subjects, 20 eyes of sub-clinical KC and 53 eyes of 39 KC patients were enrolled. The vertical thickness profiles of epithelium and Bowman's layer in each eye were measured using UHR-OCT. Eight diagnostic indices including ESD (epithelial standard deviation) and BSD (Bowman's layer standard deviation), ESV (epithelial standard variation) and BSV (Bowman's layer standard variation), EEI (epithelium ectasia index) and BEI(Bowman's ectasia index), EEI-MAX(maximum epithelial ectasia index) and BEI-MAX((maximum Bowman's ectasia index) were calculated to quantify the specific change pattern for each layer. Receiver operating characteristic (ROC) curves were used to determine the diagnostic accuracy (area under the curve, AUC) and to identify optimal cutoff points to maximize sensitivity and specificity in discriminating keratoconus and subclinical keratoconus from normal corneas.
Results: Both minimum thicknesses of epithelium and Bowman's layer were statistically thinner in KC (41.55 ± 6.42 μm for EL, 11.08 ± 2.84 μm for BL, both P< 0.005) and sub-clinical KC (49.47 ± 4.06 μm for EL, 15.44 ± 2.42 μm for BL, both P <0.05). ROC curve analyses showed high diagnostic accuracy of the indices (AUC ranged from 0.95 to 0.98, and 0.83 to 0.87, respectively) and Bowman's layer (AUC ranged from 0.91 to 0.96, and 0.71 to 0.87, respectively) for both KC and subclinical KC. Among all investigated indices based on vertical thickness profiles of epithelium and Bowman's layer, ESD provided the higher diagnostic accuracy to discriminate keratoconus (AUC 0.98 with sensitivity and specificity of 98% and 97%, respectively) and subclinical keratoconus (AUC 0.87 with sensitivity and specificity of 80% and 73%, respectively) from normal corneas.
Conclusions: UHR-OCT characterized the vertical thickness change patterns of epithelium and Bowman's layer among normal, sub-clinical KC and KC eyes. The diagnostic index of ESD detected the sub-clinical KC and KC eyes with high accuracy and it might be useful to detect early or even sub-clinical KC.
Commercial Relationships: Meixiao Shen, None; **Zhe Xu**, None; **Mei Peng**, None; **Jun Jiang**, None; **Jianhua Wang**, None; **Fan Lv**, None
Support: National Natural Science Foundation of China 81400441

Program Number: 1620 Poster Board Number: D0128
Presentation Time: 8:30 AM–10:15 AM
In Vivo Confocal Microscopy in Histologically Confirmed Small Fiber Neuropathy
Franziska Bucher[1], Christian Schneider[2], Tobias Blau[3], Claus Cursiefen[1], Gereon R. Fink[2], Helmar C. Lehmann[2], Ludwig M. Heindl[1]. [1]Department of Ophthalmology, University Hospital Cologne, Cologne, Germany; [2]Department of Neurology, University Hospital Cologne, Cologne, Germany; [3]Department of Pathology, University Hospital Cologne, Cologne, Germany.
Purpose: In patients with small fiber neuropathy (SFN) non-invasive diagnostic tests that allow accurate monitoring of disease progression are urgently needed. Aim of this study was to assess corneal trigeminal small sensory nerves and immune cells by in vivo corneal confocal microscopy (CCM) in histologically confirmed SFN.
Methods: This prospective single-center study analyzed 14 patients with histologically confirmed SFN. CCM parameters (corneal nerve fiber density (NFD), total number of nerves, number of main trunks, and branches, nerve tortuosity, and dendritic cell density (DCD)) were compared to 14 age-matched healthy controls and correlated with clinical symptoms, disease course and histopathological findings.
Results: Corneal NFD (15489.3 ± 5927.6 μm/mm² vs. 22687.1 ± 4328.7 μm/mm²; p=0.001) and total number of nerves (10.4 ± 4.6 /

frame vs. 18.5 ± 4.8 /frame; p<0.0001) were significantly reduced in patients with SFN. In contrast, nerve tortuosity was significantly increased (2.2 ± 0.31 vs. 1.7 ± 0.5; p=0.02). Corneal NFD did not correlate with intraepidermal NFD (ρ -0.158; p>0.05) or clinical measures (p>0.05). Average dendritic cell density (DCD) was increased in SFN (33.5 ± 57.5 cells/mm^2 vs. 16.1 ± 13.7 cells/mm^2), but did not reach significance (p>0.05).

Conclusions: CCM provides parameters that reliably indicate injury to sensory afferents of the trigeminal nerve in patients with SFN. Our data suggest that CCM may serve both as a non-invasive diagnostic test and a surrogate marker in SFN.

Program Number: 1621 **Poster Board Number:** D0129
Presentation Time: 8:30 AM–10:15 AM
Correlation of Multiphoton Microscopy, Tissue Morphological Changes and Enzymatic Resistance in Riboflavin-UVA Crosslinked Human Corneas

Maria Laggner[1], Ying-Ting Chen[1], Gerald Schmidinger[1], Ruth A. Byrne[2], Clemens Scheinecker[2], Marion Funk[1], Ursula Schmidt-Erfurth[1], Andreas Pollreisz[1]. [1]Department of Ophthalmology and Optometry, Medical University of Vienna, Vienna, Austria; [2]Department of Rheumatology, Medical University of Vienna, Vienna, Austria.
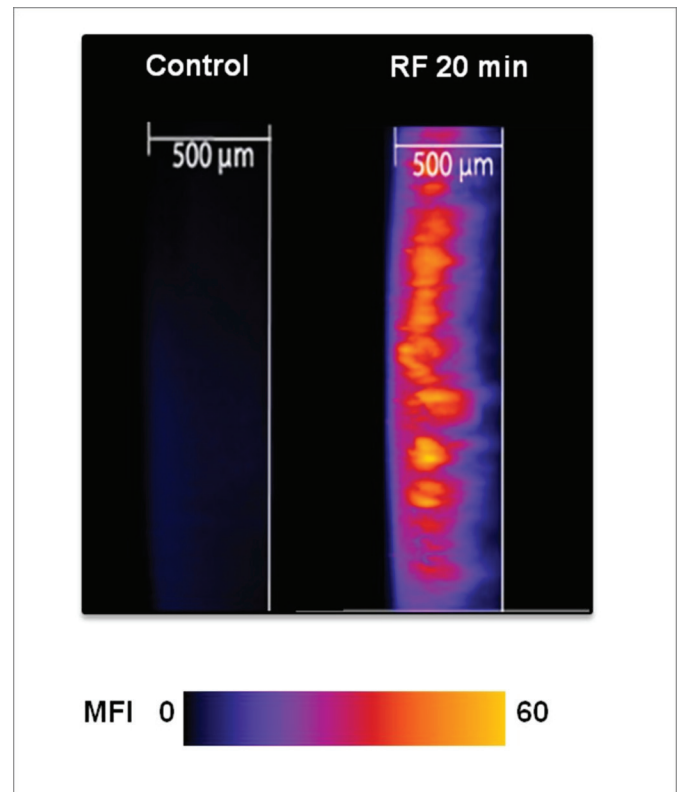
Purpose: Collagen crosslinking (CXL) is a well established procedure to treat ocular disorders with cornea ectasia, and yet today there is no standardized technique to evaluate corneal CXL in clinical settings. To explore the utility of multiphoton imaging as a non-invasive tool to assess CXL efficacy, we investigated the correlation between second harmonic generation (SHG) imaging and histological/biochemical changes of corneas after riboflavin (RF)-induced UVA CXL.

Methods: De-epithelialized human corneoscleral tissues were imaged by Leica SP5 multiphoton microscope to study (1) RF tissue diffusion profile and (2) SHG signals before and after CXL. Z-stack images were acquired throughout 500 μm of corneas with a 15 μm interslice interval. The emission of the MP laser was set to a wavelength of 800 nm. RF 0.1% was installed for 5, 10 and 20 min with 20 % Dextran vehicle as controls, followed by UVA irradiance at 3 J/cm^2. Masson's trichrome staining (MTS) and collagenase digestion assay were employed to assess the collagen ultrastructural changes and enzymatic resistibility.

Results: The corneal stromal absorption of RF was significantly higher in 20 min compared to 5 and 10 min drug instillation. Intensity of SHG signals was remarkably reduced post RF-UVA CXL at all RF instillation time points compared to dextran controls. However, correlation between RF and SHG profile was only observed in 10 and 20 min RF instillation (R^2 = 0.13 and 0.28, respectively, all *p* <.05), but not in 5 min group. In contrast to a rugged, heterogenous collagen texture of unirradiated controls, MTS revealed homogenous collagen fibril lamellae in crosslinked corneas in an RF dose-dependent manner. The intercalated collagen fibril texture in the anterior stroma was observed in all RF groups, while such a lattice structure in the posterior stromal segment was only noticed in 20

min RF group. Lastly, collagenase assay showed that tissue strength was significantly increased by higher doses of RF in UVA CXL. Histological and biochemical evaluations further suggest that the RF doses are related to the depth of CXL in the corneal stroma.

Conclusions: An RF-defined threshold determines the applicability of SHG imaging as a non-invasive technique in assessing the efficacy of RF-UVA CXL for the treatment of cornea ectasia.

Axial riboflavin diffusion profile imaged by multiphoton microscopy

Program Number: 1622 **Poster Board Number:** D0130
Presentation Time: 8:30 AM–10:15 AM
Thinnest pachymetry and nasal-temporal asymmetry in myopia and emmetropia by Pentacam

Sven Jonuscheit[1, 2], Michael J. Doughty[1], Raul Martin[3, 4], Ana Rio-Cristobal[3, 4]. [1]Vision Sciences, Dept. of Life Sciences, Glasgow Caledonian University, Glasgow, United Kingdom; [2]Institute for Applied Health Research, Glasgow Caledonian University, Glasgow, United Kingdom; [3]Departamento de Física Teórica, Atómica y Óptica, Universidad de Valladolid, Valladolid, Spain; [4]Instituto Universitario de Oftalmobiología Aplicada (IOBA Eye Institute), Universidad de Valladolid, Valladolid, Spain.

Purpose: To assess the association between thinnest point pachymetry and nasal-temporal asymmetry in healthy Caucasian individuals with myopia and emmetropia.

Methods: One hundred and four healthy prepresbyopic subjects (49 myopes, 55 emmetropes) were assessed using the Pentacam Scheimpflug system. One eye per subject and the mean of two

measurements were used for analysis. Corneal thickness was extracted from topographic maps including the apex (CCT) and peripheral nasal and temporal points up to 5 mm away from the centre. Thinnest pachymetry (TP) was recorded and the apex-to-thinnest-pachymetry difference (ATD) and apex-to-thinnest ratio (ATR) generated. Absolute nasal-temporal pachymetry differences (NTD) were calculated by subtracting temporal from corresponding nasal values. The relative peripheral asymmetry was expressed as the nasal-temporal ratio (NTR) between corresponding locations. Simple linear regression was used to assess the relationship between ATR and nasal-temporal asymmetry for all as well as myopic and emmetropic eyes.

Results: The mean age of all subjects was 24±6 years. The mean spherical equivalent was -1.43±1.95 D for all subjects, and -3.05±1.75 D and 0.01±0.19 D for the myopic and emmetropic sub-groups respectively. CCT averaged 554±32 µm and TP 550±32 µm, with a mean ATD of 4.51±2.24 µm and an ATR of 1.008±0.004. Corneal thickness increased asymmetrically with increasing distance from the apex, with a mean NTD of 58±22 µm and a mean NTR of 1.087±0.034 (at 4 mm from apex). Thinnest pachymetry was related to apex thickness (r=0.998, p<0.001). ATR was associated with NTR (r=0.485, p<0.001) and ATD with NTD (r=0.466, p<0.001). These relationships were noted for both groups of myopic and emmetropic eyes (p<0.001).

Conclusions: In normal corneas without focal thinning the difference and the ratio between apex and thinnest pachymetry are related to the nasal-temporal asymmetry. Further studies on eyes with progressive central or peripheral thinning would be useful to investigate the theory whether peripheral asymmetry is a potential driver for corneal thinning disorders and whether relationships exist between anterior and posterior segment asymmetry.

Commercial Relationships: Sven Jonuscheit, None; **Michael J. Doughty**, None; **Raul Martin**, None; **Ana Rio-Cristobal**, None
Support: Santander Universities UK

Program Number: 1623 **Poster Board Number:** D0131
Presentation Time: 8:30 AM–10:15 AM
Quantitative evaluation of refractive components of posterior corneal surface using Fourier analysis: an attempt to determine a normal range of values for each Fourier index
Yusuke Inoue, Yuta Ueno, Takahiro Hiraoka, Fumiki Okamoto, Tetsuro Oshika. Ophthalmology, Unversity of Tsukuba, Tsukuba, Japan.

Purpose: Fourier analysis has been used to quantify irregular astigmatism. Although a normal range of values has already been determined for the anterior surface of the cornea, it has not been established for the posterior surface yet. This study aims to determine the normal distribution of each refractive component of the posterior corneal surface by Fourier analysis using anterior segment OCT.

Methods: Three hundred normal eyes were enrolled in the study. The anterior/posterior corneal height data were obtained with an anterior segment Fourier-domain OCT (CASIA, TOMEY, Nagoya, Japan). Four components of the posterior corneal surface, such as spherical power, regular astigmatism, asymmetry and higher order irregularity, were calculated from the obtained data using Fourier analysis. A normal range of values was defined as the mean ± 2SD for each component. Moreover, 40 eyes with astigmatism higher than -2.00D, 50 eyes with keratoconus, 25 eyes submitted to penetrating keratoplasty, and 12 eyes submitted to DSAEK were also evaluated, and the ratio of those included within the normal range for each studied component was calculated.

Results: In normal eyes, the normal range of posterior corneal surface values was -6.60 ~-5.70D for spherical power, 0 ~ 0.27D

for regular astigmatism, 0 ~ 0.10D for asymmetry, and 0 ~ 0.03D for higher order irregularity. In pathologic corneas, the percentage of eyes included within the normal range for spherical power, regular astigmatism, asymmetry and higher order irregularity was respectively 83, 55, 90, 93 % in the high astigmatism group, 4, 8, 0, 2 %, in the keratoconus group, 25, 12, 4, 0 %, in the penetrating keratoplasty group, and 17, 42, 0, 8%, in the DSAEK group.

Conclusions: We determined, for the first time, a normal range of values for the refractive components of the posterior corneal surface using Fourier analysis. These numbers could be used for comparison purposes with pathologic corneas. Also, the ratio of keratoconic eyes showing values within the normal range was extremely low for all components in the posterior corneal surface, suggesting these measurements could be useful in the diagnosis of this pathology.

Commercial Relationships: Yusuke Inoue, None; **Yuta Ueno**, None; **Takahiro Hiraoka**, None; **Fumiki Okamoto**, None; **Tetsuro Oshika**, None

Program Number: 1624 **Poster Board Number:** D0132
Presentation Time: 8:30 AM–10:15 AM
The clinical significance of Fuchs' flecks in pterygia and pinguecula: are Fuchs' flecks an early indicator of ultraviolet light damage
Matthew H. Ip[1, 2], Jeanie J. Chui[1], Lien Tat[1, 3], Minas T. Coroneo[1, 3].
[1]Department of Ophthalmology, Prince of Wales Hospital, Randwick, NSW, Australia; [2]University of New South Wales, Sydney, NSW, Australia; [3]Ophthalmic Surgeons, Randwick, NSW, Australia.

Purpose: Fuchs' flecks (FF) have been previously identified at the leading edge of pterygia, and may represent stem-like cells that give rise to this condition. However, the frequency of occurrence of FF and their clinical significance remains undefined. We hypothesize that FF are precursor lesions that can give rise to ultraviolet light-related disorders such as pinguecula and pterygia. This study aims to evaluate the presence and clinical significance of FF in macroscopically normal eyes, pinguecula and pterygium-affected eyes.

Methods: A single center, retrospective observational case series was performed to evaluate the clinical significance of FF in ocular surface disorders such as pterygium and pinguecula by in vivo confocal microscopy (IVCM). 40 eyes from 20 patients with clinical diagnoses of pinguecula and/or pterygium in at least one eye were examined with IVCM (Rostock Cornea Module; Heidelberg Engineering Heidelberg, Germany). The main outcome measure was the presence of FF in patients with pinguecula and/or pterygium. Macroscopically normal paired eyes were also examined with IVCM to determine FF presence. Descriptive statistics were used to determine the percentage and frequency of FF in different limbal regions.

Results: FF were present in 30 of 37 (81.1%) macroscopically normal nasal or temporal limbal regions, 12 of 12 (100%) pinguecula, 13 of 15 (86.7%) primary pterygia, and 8 of 8 (100%) of recurrent pterygia. No FF could be identified at the superior or inferior limbal regions.

Conclusions: High rates of FF were identified at the advancing head of pinguecula, primary pterygium, recurrent pterygium and in the macroscopically normal nasal and temporal limbal regions of the second eye in patients with unilateral disease. This suggests that FF may represent precursor lesions to ultraviolet-associated ocular surface pathology. The use of IVCM to identify FF may consequently permit clinicians to earlier diagnose and predict recurrence of pterygium and onset of pinguecula.

Commercial Relationships: Matthew H. Ip, None; **Jeanie J. Chui**, Genetic Eye Foundation (F); **Lien Tat**, None; **Minas T. Coroneo**, None

Program Number: 1625 **Poster Board Number:** D0133
Presentation Time: 8:30 AM–10:15 AM
A Comparison of the Casia SS-1000 Keratometry and Atlas 9000 SimK Topography Values
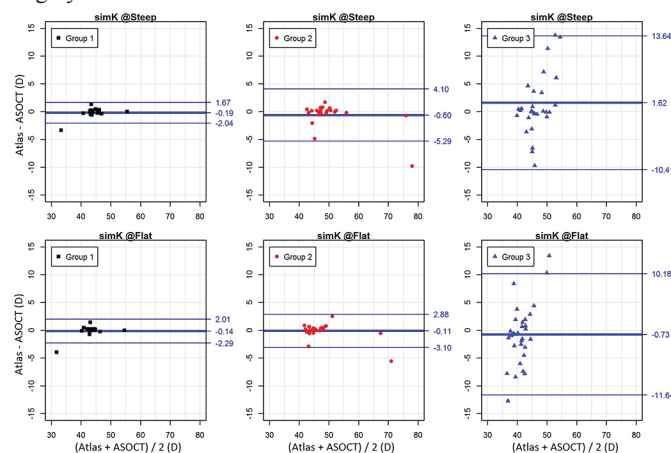*Christopher M. Pruet[2, 1], Kanwal Matharu[2], Alice Chuang[2], Gene Kim[2, 1].* [1]Robert Cizik Eye Clinic, Houston, TX; [2]Ruiz Department of Ophthalmology and Visual Science, The University of Texas Medical School at Houston, Houston, TX.
Purpose: To determine the agreement of keratometry measured by the CASIA SS-1000 Anterior Segment Ocular Coherence Tomography (ASOCT; Tomey, Nagoya, Japan) with SimK values measured by Atlas 9000 (Carl Zeiss Meditec, Dublin, CA).
Methods: : A retrospective chart review was performed of patients who had undergone both ASOCT 'Corneal Map' mode imaging and ATLAS topography. Eyes were excluded if they had anterior segment abnormalities precluding topography measurements. If both eyes were eligible, one eye was randomly selected. Demographics were recorded. Eyes were classified into three groups based on the ocular history: eyes without corneal diseases (group 1), eyes with keratoconus (KCN) or pellucid marginal degeneration (PMD) (group 2), and eyes with prior corneal surgery (group 3). Bland-Altman agreement plot was used to evaluate the mean difference between ASOCT and Atlas and limits of agreement.
Results: Seventy-one eyes were included. The mean age was 46.8 (± 19.1) years with 31 (43.7%) male, 35 (49.3%) White, 18 (25.4%) Black and 10 (14.1%) Hispanics and 36 (50.7%) right eyes. Seventeen eyes (23.9%) were in group 1, 29 (40.8%) in group 2 and 25 (35.2%) in group 3. Previous corneal surgeries included 7 (9.9%) Descemet's stripping automated endothelial keratoplasty (DSAEK), 16 (22.5%) full thickness penetrating keratoplasty (PKP), and 2 (2.8%) LASIK. Figure 1 showed Atlas keratometry readings average 0.19 D lower, 0.60D lower, and 1.62D higher for the steep measurements in groups 1, 2, and 3 respectively, and 0.14 D lower, 0.11 lower, 0.73 D lower for groups 1, 2, and 3 for flat measurements. The limits of agreement showed a 95% variation within 1.85D, 4.7D and 12.02 D on steep keratometry for groups 1, 2, and 3 respectively, and 2.15 D, 3.00 D, and 10.91 D on flat keratometry for groups 1, 2, and 3 respectively.
Conclusions: There is generally good agreement between the Casia SS-1000 and the Atlas 9000 topographies when eyes are without prior surgery or ectatic disease. Agreement between the devices decreased somewhat with ectasic disease and substantially with prior corneal surgery.

Program Number: 1626 **Poster Board Number:** D0134
Presentation Time: 8:30 AM–10:15 AM
Corneal radius of curvature measurements in normal and post-refractive surgery eyes using point-source color LED and dual-Scheimpflug Placido topographer
Eric J. Kim, Ildamaris Montes de Oca, Li Wang, Mitchell Weikert, Sumitra Khandelwal, Zaina Al-Mohtaseb, Douglas D. Koch. Ophthalmology, Cullen Eye Institute, Baylor College of Medicine, Houston, TX.
Purpose: To report anterior and posterior corneal radius of curvature (ROC) measurements with point-source color LED and dual-Scheimpflug Placido topographers in normal and post-refractive surgery eyes.
Methods: In this prospective comparative study, a single observer performed three consecutive measurements in one eye of each subject using the Cassini point-source color LED topographer (i-Optics) and the Galilei dual-Scheimpflug Placido tomographer (Ziemer). The anterior and posterior corneal ROC was measured in the following groups: (1) normal, (2) myopic post-refractive surgery, and (3) post-radial keratotomy (RK) eyes. For each group, the minimum and maximum anterior/posterior ROC ratios were used to calculate the theoretical minimum and maximum posterior corneal power given a measured anterior corneal ROC. The variability in the theoretical posterior corneal power was calculated as the difference between the theoretical minimum and maximum values.
Results: In patients analyzed to date, the anterior/posterior ROC ratio as measured by the Galilei was 1.20 ± 0.02, 1.28 ± 0.06, and 1.13 ± 0.11 in normal (n=34), post-refractive (n=21), and post-RK (n=6) eyes, respectively. The ratio as measured by the Cassini was 1.19 ± 0.03, 1.25 ± 0.05, and 1.27 ± 0.05 in normal, post-refractive, and post-RK eyes, respectively. The variability of the theoretical posterior corneal power as measured by the Galilei was 0.49 ± 0.02 D, 1.16 ± 0.06 D, and 1.29 ± 0.06 D in normal, post-refractive, and post-RK eyes, respectively. The variability as measured by the Cassini was 0.52 ± 0.02 D, 0.89 ± 0.06 D, and 0.49 ± 0.04 D in normal, post-refractive, and post-RK eyes, respectively. These results are presented in Tables 1 and 2.
Conclusions: Preliminary results suggest that the variability in the anterior/posterior ROC ratio may help explain part of the error in intraocular lens calculations when a fixed ratio is assumed. Final results and conclusions will be presented.

Commercial Relationships: Christopher M. Pruet, None; **Kanwal Matharu**, None; **Alice Chuang**, None; **Gene Kim**, None

	Anterior/Posterior ROC Ratio	
	Galilei	Cassini
Normal		
Mean ± SD	1.20 ± 0.02	1.19 ± 0.03
Range	[1.16 – 1.25]	[1.15 – 1.25]
Post-refractive		
Mean ± SD	1.28 ± 0.06	1.25 ± 0.05
Range	[1.18 – 1.42]	[1.17 – 1.35]
Post-RK		
Mean ± SD	1.13 ± 0.11	1.27 ± 0.05
Range	[0.94 – 1.22]	[1.21 – 1.32]

RK = radial keratotomy; ROC = radius of curvature; SD = standard deviation

Table 1. Ratio of anterior and posterior radius of curvature in normal, post-refractive surgery, and post-radial keratotomy patients as measured by the Galilei and the Cassini.

	Theoretical Posterior Corneal Power Variability (D) (Mean ± SD)	
	Galilei	Cassini
Normal	0.49 ± 0.02	0.52 ± 0.02
Post-refractive	1.16 ± 0.06	0.89 ± 0.06
Post-RK	1.29 ± 0.06	0.49 ± 0.04

D = diopter; RK = radial keratotomy, SD = standard deviation

Table 2. Variability of theoretical posterior corneal power in normal, post-refractive surgery, and post-radial keratotomy patients as measured by the Galilei and the Cassini.

Commercial Relationships: Eric J. Kim, None; **Ildamaris Montes de Oca**, None; **Li Wang**, Ziemer (R); **Mitchell Weikert**, Ziemer (C); **Sumitra Khandelwal**, None; **Zaina Al-Mohtaseb**, None; **Douglas D. Koch**, Abbott Medical Optics (C), Alcon Laboratories, Inc (C), i-Optics (C), Ziemer (C)

Program Number: 1627 **Poster Board Number:** D0135
Presentation Time: 8:30 AM–10:15 AM
Clinical Comparison of Keratometry Measurements between Automated Keratometer and Placido-Rings Based Topographer
Kevin Yum[1, 2], Dorothy Pham[1, 2], Ahmad Al-Heeti[1], Jenny Baek[1, 2], Samir I. Sayegh[1]. [1]The Eye Center, Champaign, IL; [2]University of Illinois at Urbana-Champaign, Urbana, IL.
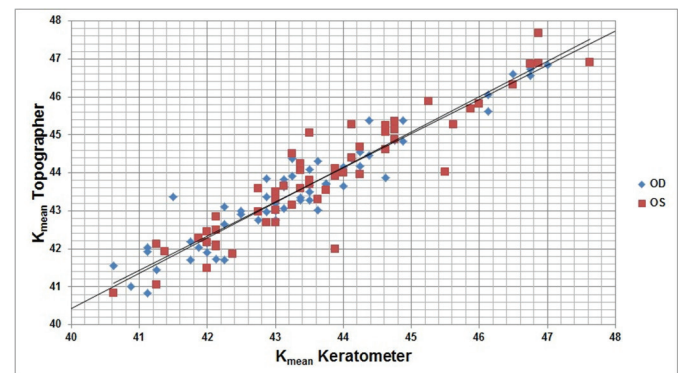**Purpose:** To compare keratometry (K) measurements and orientation of pre-operative cataract patients between the automated keratometry and Placido-rings based topography devices.
Methods: K-values of 55 pre-operative cataract patients (with a total of 61 eyes), ages ranging from 46 to 89 with the mean age of 68, were obtained using an automated keratometer (Humphrey Zeiss 599) and a Placido-rings based topographer (Topcon CA-200F). All patients were sequentially tested with the automated keratometer followed by the Placido-rings based topographer on the same day in order to minimize variability. Mean, standard deviation, and Lin's concordance correlation coefficients (Lin et al. 2002) were calculated, and correlation graphs were plotted and analyzed. Each graph consisted of equivalent K-values obtained from both the

keratometry and topography devices on two separate axes. Based on the Cataract Surgery Guidelines established by the Royal College of Ophthalmologists, we created an exclusion criterion for cataract patients with △K and orientation differences larger than ±1 diopter and ±20 degrees.
Results: Our preliminary data demonstrated that inter-device concordance correlations were higher in K_{flat} (ρ_{OD}=0.9235, ρ_{OS}=0.9371), K_{steep} (ρ_{OD}=0.9508, ρ_{OS}=0.9017), and K_{mean} (ρ_{OD}=0.9467, ρ_{OS}=0.9359) than in variables relevant to the computation of toric intraocular lenses, for example, K_{steep}-orientation (ρ_{OD}=0.8867, ρ_{OS}=0.5894). 33 out of 61 patients met the criterion defined above.
Conclusions: While determining the correct K_{mean} measurement is important for proper spherical intraocular lens (spherical IOL) calculation, additional corneal astigmatism (△K; $K_{steep} - K_{flat}$) and orientation or axis measurements are required for toric IOL calculation. Our moderately low inter-device concordance results prompt further experiments to test for the cause of discrepancy. Based on this preliminary analysis, we recommend a third keratometry device such as the IOL Master for better analysis and IOL power calculation.

K_{mean} Topography vs. K_{mean} Keratometer
Commercial Relationships: Kevin Yum, None; **Dorothy Pham**, None; **Ahmad Al-Heeti**, None; **Jenny Baek**, None; **Samir I. Sayegh**, None

Program Number: 1628 **Poster Board Number:** D0136
Presentation Time: 8:30 AM–10:15 AM
Clinical comparison of keratometry measurements between IOL Master vs automated keratometer and IOL Master vs Placido-based topographer
Ahmad Al-Heeti[1], Kevin Yum[2], Dorothy Pham[3], Samir I. Sayegh[1]. [1]The Eye Center, Champaign, IL; [2]Biochemistry, University of Illinois at Urbana-Champaign, Champaign, IL; [3]Molecular and Cellular Biology, University of Illinois at Urbana-Champaign, Champaign, IL.
Purpose: To compare keratometry measurements and orientation of pre-operative cataract patients using the IOL Master to to automated keratometry and placido-based topography devices.
Methods: K-values of 47 eyes from pre-operative cataract patients, ages ranging from 46 to 90 mean age of 69, were obtained using the IOL Master (IOL Master 500), automated keratometer (HumphreyZeiss 599) and the placido-based topographer (Topcon CA-200F). All patients were sequentially tested with the keratometer followed by the topographer and IOL Master on the same day in order to minimize variability. Mean and standard deviation were calculated, and various keratometry correlation graphs were plotted and analyzed. Each graph consists of equivalent K-values obtained from the IOL master vs keratometer and IOL master vs topographer devices on two separate axes. All correlation coefficients were

calculated based on mean and standard deviation obtained from various K-values.

Results: Our preliminary data demonstrate that there were good concordance correlation coefficient in flat K (CCC_{OD}= 0.9528, CCC_{OS}= 0.9631) and (CCC_{OD}= 0.9097, CCC_{OS}= 0.9344), steep K (CCC_{OD}= 0.9515, CCC_{OS}= 0.9277) and (CCC_{OD}= 0.9128, CCC_{OS}= 0.9517), and mean K (CCC_{OD}= 0.9665, CCC_{OS}= 0.9586) and (CCC_{OD}= 0.9197, CCC_{OS}= 0.9565) for IOL master vs keratometer and IOL master vs topographer devices respectively, and also flat K-orientation (CCC_{OD}= 0.9177, CCC_{OS}= 0.871) for IOL master vs keratometer. CCC for variables relevant to toric lenses computations had slightly lesser values. For example ftat K-orientation for IOL master vs topographer was (CCC_{OD}= 0.8923, CCC_{OS}= 0.8026).

Conclusions: As optical biometry becomes a gold standard relied upon for IOL power calculation, it is important to characterize its concordance with instruments that have been relied on for decades. This study takes a step in this direction, illustrating the methods and some preliminary conclusions.

Commercial Relationships: Ahmad Al-Heeti, None; **Kevin Yum**, None; **Dorothy Pham**, None; **Samir I. Sayegh**, None

Program Number: 1629 **Poster Board Number:** D0137
Presentation Time: 8:30 AM–10:15 AM
Cross-linking Wound Healing In Animal Models: A Complementary Study Using Two-photon Microscopy And Histological Analysis
Carmen Martinez-Garcia[1], Francisco J. Avila[2], Lucía Ibares-Frías[3], Raquel Palacios[2], Patricia Gallego-Muñoz[1], Roberto Cantalapiedra[1], Juan M. Bueno[2]. [1]Cell Biology, University of Valladolid, Valladolid, Spain; [2]Laboratorio de Optica, Universidad de Murcia, Murcia, Spain; [3]Oftalmologia, Hospital Clinico Universitario, Valladolid, Spain.

Purpose:
To analyze and compare the wound healing after cross-linking (CXL) treatment in two animal models (hens and rabbits) using second harmonic generation (SHG) microscopy imaging and histological analysis.

Methods: Monolateral CXL treatment was performed on 10 rabbits and 10 hens. The central 7-mm of the corneal epithelium was removed and 0.125% riboflavin+20% dextran solution was instilled during 30 minutes, then every 5 min during of UVA radiation. The eye was illuminated with UV-light (370 nm, 3 w/cm^2) during 30 minutes. Animals were euthanized after 30 days of CXL treatment, the eyes enucleated and the corneas excised. The unstained ex-vivo corneas were imaged using a custom two-photon microscope (Bueno et al., 2010), which allows optical sectioning. Later, a histological analysis was done under bright-field microscopy after hematoxylin-eosin staining. Treated and contralateral corneas were compared using both techniques

Results: SHG images showed sets of collagen bundles running parallel to each other with some orthogonal interweaving. One month after the CXL treatment, central and posterior stromal organization seemed not to be affected by the treatment. However, for the anterior stroma the effects of CXL differed between hens and rabbits. In the former, the collagen distribution recovered its usual arrangement and did not differ from control corneas. In rabbits, this part of the stroma presented changes that remain one month after CXL treatment. Collagen bundles lost their regular orientation and appeared less delineated and less interwoven after CXL compared to the control samples. Histology from hens showed corneas depleted of cells in the anterior stroma and light hipercellularity in the medium stroma. In rabbits, treated corneas were similar to control.

Conclusions: The wound healing after CXL was different in both animal models. SHG imaging and histological analyses provided complementary information on corneal structures: collagen organization and cell distribution respectively. The former revealed that the regular stromal arrangement was recovered faster in hens than in rabbits. The later showed that the cellular repopulation was slower in chickens than in rabbits.

Commercial Relationships: Carmen Martinez-Garcia, None; **Francisco J. Avila**, None; **Lucía Ibares-Frías**, None; **Raquel Palacios**, None; **Patricia Gallego-Muñoz**, None; **Roberto Cantalapiedra**, None; **Juan M. Bueno**, None
Support: Spanish Government Grant, MINECO, FIS2011-25637

Program Number: 1630 **Poster Board Number:** D0138
Presentation Time: 8:30 AM–10:15 AM
Quantitative ultrasound mapping of the corneal stroma
Suzanne Daly[1], Ronald H. Silverman[1, 2], Raksha Urs[1], Harriet Lloyd[1], Mara Berganovsky[1], Winston Kung[1]. [1]Ophthalmology, Columbia University Medical Center, New York, NY; [2]Lizzi Center for Biomedical Imaging, Riverside Research, New York, NY.

Purpose: The organization of stromal collagen and keratocyte distribution may be altered in corneal disease (e.g., keratoconus) and following crosslink therapy. Because of such alterations, changes in optical and ultrasound backscatter within the stroma might be expected. We report here a novel approach to characterization and display of stromal microstructural changes via quantitative ultrasound analysis.

Methods: We used a 60 MHz transducer with a 2-mm aperture and 6-mm focal length. We initially scanned rabbits (8 eyes) pre-and post-crosslinking, acquiring 3D rectilinear sets of 200 scans at 10-mm intervals. We then adapted the system to scan human subjects using an immersion setup with arc-shaped scan geometry matched approximately to the radius of the human cornea. Phase-resolved data were acquired in 6 radial planes at 30-degree intervals over a 5.5 mm diameter region. We generated spectral parameter images of the stroma representing spectral slope (dB/MHz), 0-MHz intercept (dB) and midband fit (dB) by using a sliding window approach such that the analysis window was approximately 5 wavelengths axially by 5 vectors laterally (approximately one beamwidth). We then performed radial interpolation to produce maps of spectral parameters representing mean spectral parameters over the full stromal depth, or over selectable depth ranges.

Results: Cross-linked rabbit corneas showed variable change in backscatter and frequency-dependence; however, changes in midband backscatter and spectral slope (dB/MHz) were correlated with corneal thickness change. Initial results in human eyes demonstrated higher backscatter in the anterior stroma in the normal cornea, even after compensation for attenuation. The acquisition of 3D data in the rabbit eye and in humans allowed generation of *en face* images, mapping backscatter parameters as a function of position and depth-range.

Conclusions: Alteration of stromal organization by disease or therapy may result in optical backscatter changes detectable by Scheimpflug, OCT or high-frequency ultrasound. The 60 MHz probe used in this study is more sensitive to small tissue inhomogeneities than UBM probes typically operating in the 35-40 MHz range. Also, ultrasound is sensitive to acoustic impedance rather than optical refractive index, and thus is complementary to optical methods. *En face* depth-wise display of stromal acoustic backscatter offers a new means for assessment of corneal disease and therapy.

Commercial Relationships: Suzanne Daly, None; **Ronald H. Silverman**, None; **Raksha Urs**, None; **Harriet Lloyd**, None; **Mara Berganovsky**, None; **Winston Kung**, None

Program Number: 1631 **Poster Board Number:** D0139
Presentation Time: 8:30 AM–10:15 AM
Evaluation of topographic indices in Hispanic patients with Keratoconus and Keratoconus suspects

Lorena Lam Franco[1], Paloma Lopez[1], Julio C. Hernandez[2], Jorge E. Valdez[2]. [1]Ophthalmology, Escuela de Medicina del Tecnológico de Monterrey, Monterrey, Mexico; [2]Ophthalmology and Visual Science Research Chair, Escuela de Medicina del Tecnológico de Monterrey, Monterrey, Mexico.

Purpose: To describe the demographic characteristics and topographic patterns of Hispanic patients with keratoconus (KC) and KC suspects.
Methods: Retrospective, observational case series. A random sample of 550 records from patients referred to the Cornea and Refractive Surgery Service from the Institute of Ophthalmology at the Zambrano Hellion Medical Center from January 2008 to November 2014. Patients diagnosed with KC or KC suspect were included for analysis. Corneal topography was performed using the Tomey Topographic Modeling System (TMS), as well as ultrasonic pachymetry to measure central corneal thickness (CCT). Analyzed topographic indices were Surface Asymmetry Index, Opposite Sector Index, Irregular Astigmatism Index, Differential Sector Index, Center/Surround Index, Keratoconus Prediction Index, and Standard Deviation of corneal Power. Posteriorly eyes were grouped into KC and KC suspect.
Results: From the entire study sample, a total of 33 patients (62 eyes) with KC/KC suspect were diagnosed. 66.7% had KC in both eyes, 21.2% KC + KC suspect, and 12.1% KC suspect both eyes. 47 eyes (4.3%) were diagnosed with KC and 15 (1.4%) as KC suspects. 20 (60.6%) were male and 13 (39.5%) female. The mean age at diagnosis was 32.8±13.22 years (range 17-64). Mean age was significantly lower in patients with KC compared to KC suspect (29.7±9.2 and 53.3±15.3 respectively, $P<0.001$). The most common cone location was central (31.9%) and 46.8% of the eyes were stage 1 in the Amsler Krumeich Classification. Eyes in the KC group had higher maximum keratometry (55.11±4.9D) and mean keratometry (48.0±7.8D), but lower CCT (498.8±43.11μm) than KC suspects (48.49±3.27D, 45.48±1.78D, and 546.4±17.07μm respectively) ($P<0.001$, $P=0.23$ and $P=0.01$). The means of the seven topographic indices were found to be significantly higher in eyes in the KC group than the KC suspect group ($P<0.001$).
Conclusions: We found an important prevalence of KC and KC suspects (4% and 1%) among our population, with a significant difference of topographic indices, age, maximum keratometry and CCT between KC suspects and KC patients.
Commercial Relationships: Lorena Lam Franco, None; **Paloma Lopez**, None; **Julio C. Hernandez**, None; **Jorge E. Valdez**, None

Program Number: 1632 **Poster Board Number:** D0140
Presentation Time: 8:30 AM–10:15 AM
Corneal epithelial remodeling as a diagnostic tool for keratoconus: A comparison of 3-D Anterior Segment OCT in a large cohort of keratoconic and normal eyes

Talia R. Kaden[1], Laurence T. Sperber[1], George Asimellis[2], A. John Kanellopoulos[1, 2]. [1]Ophthalmology, New York University, New York, NY; [2]The Laservision.gr Research & Clinical Eye Institute, Athens, Greece.

Purpose: To use anterior-segment optical coherence tomography (AS-OCT) to investigate epithelial thickness distribution characteristics in keratoconic patients

Methods: The study group (A) consisted of 160 eyes with clinically diagnosed keratoconus and the control group (B) was composed of 160 non-keratoconic eyes. Employing anterior-segment OCT (RtVue-100, Optovue, Fremont, CA), three successive acquisitions were performed in each eye. 3-dimensional epithelial thickness maps were obtained, enabling investigation of epithelial thickness at the pupil center, mid-periphery, superior and inferior cornea. These data provided the average, maximum, minimum, and topographic epithelial thickness variability. Intra-individual variation of epithelial thickness measurement was also evaluated. We further investigated correlation of the epithelial data via newly defined Scheimpflug imaging–derived anterior-surface irregularity indices for keratoconus severity: the index of height decentration (IHD) and the index of surface variance (ISV). The epithelial thickness indices were then correlated with these two indices.
Results: The average intra-individual epithelial thickness repeatability was 1.67μm in Group A (keratoconic group) and 1.13μm in Group B (control group). The pupil center epithelial thickness was 51.75±7.02 μm in the keratoconic group, and maximum and minimum thickness were 63.54±8.85 μm and 40.73±8.51 μm. In the control group, epithelial thickness at the center was 52.54±3.23 μm, maximum thickness was 55.33±3.27 μm and the minimum was 48.50±3.98 μm. Topographic variability was 6.07±3.55 μm in the keratoconic group, while 1.59±0.79 μm in the control group. Both epithelial thickness variability and range, defined as minimum-maximum, correlated tightly with the indices of IHD and ISV.
Conclusions: AS-OCT offers both ease of use and high predictability in assessing in-vivo epithelial thickness measurement in keratoconus. We have demonstrated that keratoconic eyes have an increased overall epithelial thickness as compared to normal eyes and that there exists a tight correlation between increased topographic thickness variability and range and keratoconus severity. Because epithelial thickness as measured by AS-OCT may be used to identify and assess mild and suspected cases of keratoconus, this technique is of particular clinical importance.
Commercial Relationships: Talia R. Kaden, None; **Laurence T. Sperber**, None; **George Asimellis**, None; **A. John Kanellopoulos**, Alcon (R), Allergan (R), iOptics (R), Keramed (R)

Program Number: 1633 **Poster Board Number:** D0141
Presentation Time: 8:30 AM–10:15 AM
Quantification of Keratoconic Focal Thinning on Corneal Epithelial Thickness Maps by Fitting of Gaussian Waveform

Maolong Tang, Yan Li, David Huang. Casey Eye Institute, Oregon Health and Science University, Portland, OR.

Purpose: To quantify the location and dimension of corneal focal thinning for eyes with keratoconus by fitting Gaussian waveform to corneal epithelial thickness maps and compared the results with the fitting to pachymetry and mean curvature maps.
Methods: All keratoconic eyes had abnormal corneal topography and more than one slit lamp signs. Normal eyes seeking LASIK surgery were used as control. Corneal pachymetry and epithelial thickness maps were obtained from a commercial Fourier-domain OCT system. Mean curvature maps were provided by Placido topography. All maps were normalized by dividing the normal reference (average map of normal eyes). Peak location, magnitude and width of the focal thinning (cone) were estimated by maximizing the cross-correlation coefficient between the normalized map and the Gaussian waveform.
Results: The study included 21 keratoconic eyes and 17 normal eyes. On the epithelial maps, the keratoconus group had higher average cross-correlation coefficient with Gaussian waveform (0.72) than that for the normal group (0.63). The average peak location

was more inferior for keratoconic eyes than that for normal eyes. <span style="line-height:20.7999992370605px">The average cone magnitude greater for keratoconus eyes (0.23 ± 0.12) than that for normal eyes (0.043± 0.018, P < 0.0001).

Conclusions: Gaussian fitting on the epithelial thickness maps, as well as pachymetry and mean curvature maps. provides an estimate of the typical location and dimension of focal thinning caused by keratoconus. Combining these parameters from different maps might be helpful in improving the diagnosis of forme fruste keratoconus.
Commercial Relationships: Maolong Tang, Optovue Inc. (F), Optovue Inc. (P); **Yan Li**, Optovue Inc. (F), Optovue Inc. (P); **David Huang**, Carl Zeiss Meditec (P), Optovue Inc. (F), Optovue Inc. (I), Optovue Inc. (P)
Support: This study was supported by NIH grants R01 EY018184, a grant from Optovue Inc. and a grant from Research to Prevent Blindness.
Clinical Trial: NCT02109848

Program Number: 1634 **Poster Board Number:** D0142
Presentation Time: 8:30 AM–10:15 AM
Features of keratoconic corneal anatomy observed with multiple imaging modalities and histology
Felipe Andreiuolo[1], Kate Grieve[1, 2], Cristina Georgeon[1, 2], Michel Paques[1, 2], Vincent M. Borderie[1, 2]. [1]Quinze Vingts National Ophtalmology Hospital, Paris, France; [2]Vision Institute, UPMC Université Paris 06, UMR_S 968 / INSERM, U968 / CHNO des XV-XX / CNRS, UMR_7210, Paris, France.
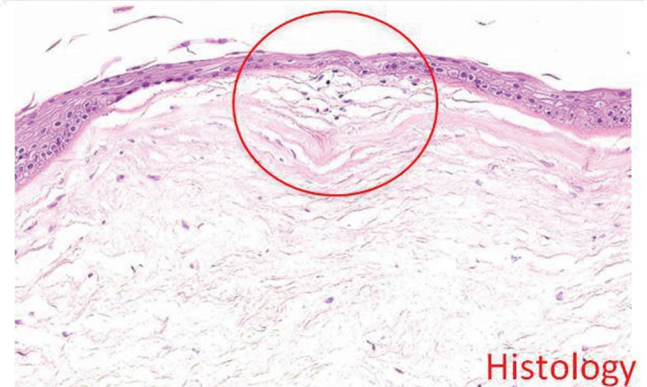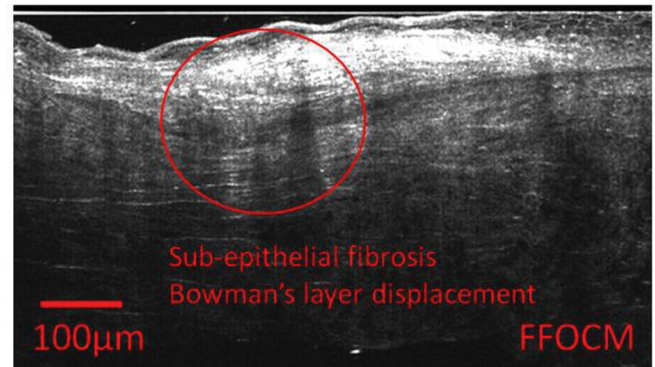**Purpose:** This study compared the anatomic appearance of keratoconic corneas using three different imaging modalities and histology.
Methods: Prospective observational study. 12 keratoconic corneas, 4 corneas with stromal scar after infectious keratitis and 8 normal corneas from human donors were examined. Stromal scars were included as this condition can be misdiagnosed as keratoconus. Patients were imaged using spectral domain optical coherence tomography (OCT, Optovue) and *in vivo* laser scanning confocal microscopy (HRTII, Heidelberg) during pre-operative examinations preceding keratoplasty. Following transplantation, the removed corneal button was imaged *ex vivo* with full-field optical coherence microscopy (FFOCM, LLTech, France). The cornea was then fixed and sent for histology. Normal human donor corneas were imaged with FFOCM for comparison with the keratoconus and scar samples.
Results: FFOCM showed good low power view detail without artifacts from histological processing such as dissociation of collagen lamella and separation of the epithelium. Corneal structural changes related to keratoconus were noted for each patient and with each imaging modality according to the 5 stages proposed by by Sandali et al (Ophthalmology, 120:12 2013): (1: thinning of epithelial and stromal layers 2: hyperreflective anomalies at the Bowman's layer (BL) and epithelial thickening 3: posterior displacement of the hyperreflective structures at BL, increased epithelial thickening and stromal thinning 4: pan-stromal scar 5: hydrops; 5a: acute onset - Descemet's membrane (DM) rupture/dilaceration of collagen lamellae and large intrastromal cysts; 5b: healing stage - pan-stromal scarring with DM rupture). Additional criteria were added based on FFOCM views, for example, BL dehiscence and sub-epithelial fibrosis, observed in 4 stage 3 subjects, with BL displaced towards the stroma, indicating that the thinned stroma at stage 3 is compensated by thickened epithelium or sub-eptihelial fibrosis. Some aspects were

more easily visible with FFOCM than histology, in particular fibrosis, Vogt's striae and keratocyte organization. Scar samples showed fewer epithelial changes in comparison to keratoconus.
Conclusions: A classification of keratoconic corneas based on imaging with OCT, HRTII, FFOCM and histology is proposed, adding new criteria based on FFOCM views, which offer artifact-free images with good morphological detail.

Sub-epithelial fibrosis
Bowman's layer displacement
100μm   FFOCM

Histology

Commercial Relationships: Felipe Andreiuolo, None; **Kate Grieve**, None; **Cristina Georgeon**, None; **Michel Paques**, None; **Vincent M. Borderie**, None

Program Number: 1635 **Poster Board Number:** D0143
Presentation Time: 8:30 AM–10:15 AM
Imaging of corneal sub-basal whorl-like nerve plexus in diabetes patients using *in vivo* corneal confocal microscopy
Tsugiaki Utsunomiya[1], Taiji Nagaoka[1], Kazuomi Hanada[2], Tsuniaki Omae[1], Harumasa Yokota[1], Akitoshi Yoshida[1]. [1]Ophthalmology, Asahikawa Medical university, Asahikawa, Japan; [2]Department of Medicine and Engineering - Combined Research Institute, Asahikawa Medical university, Asahikawa, Japan.
Purpose: Non-invasive and repeated imaging of the corneal sub-basal nerve plexus is made possible by *in vivo* corneal confocal microscopy (CCM). This diagnostic technique can be used to monitor the status of neuropathy in diabetes patients because the corneal nerve plexus decreases with the progression of diabetic neuropathy. However, it is unclear which part of the sub-basal nerve plexus around the central cornea is captured by CCM, which may induce measurement errors when data are compared between patients or over time in the same patient. There is a whorl-like characteristic pattern of corneal sub-basal nerve plexus in the infero-central cornea and we examined the CCM images of the whorl-like patterns in patients with diabetes.
Methods: A total of 19 diabetes patients and 7 healthy control subjects were examined by CCM to compare the characteristics of

the corneal sub-basal nerve plexus around the center of the cornea (conventional method) and the whorl-like pattern in the infero-central cornea (study method) by using a Rostock Corneal Module/ Heidelberg Retina Tomograph . The five clearest images of the sub-basal nerve plexus around the central cornea and the best image of the whorl-like nerve plexus in the infero-central cornea were selected for further analysis. Nerve analysis was carried out using Neuron J to measure the total corneal nerve fiber and branch length (CNFL) in addition to corneal nerve fiber and branch density (CNFD).

Results: Total CNFL were significantly shorter in the DM group compared to the control group in both conventional and whorl-like methods (p = 0.0039 vs. p = 0.0047). We confirmed a significant decreasing trend of total CNFL with the progression of diabetes retinopathy, nephropathy, neuropathy, and the loss of corneal sensation. There was also significant correlation between conventional CNFL and whorl-like CNFL (r = 0.790, p < 0.0001). CNFL measured by the whorl-like method were significantly longer than that measured in conventional CNFL in healthy subjects and diabetes patients.

Conclusions: As the whorl-like pattern is a characteristic structure of the infero-central cornea and whorl-like CNFL has the same decreasing trend as conventional CNFL, measurements of the whorl-like patterns in the corneal sub-basal nerve plexus would be more suitable for monitoring diabetic peripheral neuropathy compared with measurements by the conventional method.

Commercial Relationships: Tsugiaki Utsunomiya, None; **Taiji Nagaoka**, None; **Kazuomi Hanada**, None; **Tsuniaki Omae**, None; **Harumasa Yokota**, None; **Akitoshi Yoshida**, None

Program Number: 1636 **Poster Board Number:** D0144
Presentation Time: 8:30 AM–10:15 AM
Local variability of parameters for characterization of the corneal sub-basal nerve
Plexus

Oliver Stachs[1], Karsten Winter[1, 2], Patrick Scheibe[2], Bernd köhler[3], Stephan Allgeier[4], Rudolf F. Guthoff[1]. [1]Department of Ophthalmology, University of Rostock, Rostock, Germany; [2]Translational Centre for Regenerative Medicine, University of Leipzig, Leipzig, Germany; [3]Institute for Applied Computer Science, Karlsruhe Institute of Technology, Karlsruhe, Germany; [4]Institute for Applied Computer Science/Automation, Karlsruhe Institute of Technology, Karlsruhe, Germany.

Purpose: The corneal sub-basal nerve plexus (SNP) offers high potential for early diagnosis of peripheral neuropathy. Changes in sub-basal nerve fibers can be assessed in vivo by confocal laser scanning microscopy (CLSM) and quantified using specific parameters. While current study results agree regarding parameter tendency, there are considerable differences in terms of absolute values. The aim of this study is to find indications for this high parameter variability.

Methods: We used a novel method of software-based large-scale reconstruction that provided SNP images from three healthy subject's central corneas, decomposed the image areas into all possible image sections corresponding to the size of a single conventional CLSM image (0.16 mm^2) and calculated a set of parameters for each image section. In order to carry out a large number of virtual examinations within the reconstructed image areas an extensive simulation procedure (10,000 runs per image) was implemented.

Results: The three analyzed images had a size of 3.75 mm^2 to 4.27 mm^2. The spatial configuration of the sub-basal nerve fiber networks varied greatly across the cornea and thus caused heavily location-dependent results as well as high value ranges for the assessed parameters. Distributions of SNP parameter values greatly varied

between the three images and showed significant differences between all images for every calculated parameter (all p < 0.001).

Conclusions: The high parameter variability contributes to the relatively small size of the conventionally evaluated SNP area in regard to the size of SNP features. Averaging of parameter values based on multiple CLSM frames does not necessarily result in good approximations of the respective reference values of the whole image area. This illustrates a potential examiner bias when selecting SNP images in the central corneal area.

Commercial Relationships: Oliver Stachs, None; **Karsten Winter**, None; **Patrick Scheibe**, None; **Bernd köhler**, None; **Stephan Allgeier**, None; **Rudolf F. Guthoff**, None

Program Number: 1637 **Poster Board Number:** D0145
Presentation Time: 8:30 AM–10:15 AM
Quantitative Analysis of Corneal Sub-basal Nerve Plexus and Inflammatory Cells in Large-area Mosaics Obtained by In Vivo Confocal Microscopy

Reza A Badian[1, 2], Tor P. Utheim[2, 3], Stephan Allgeier[4], Bernd köhler[4], Alfredo Ruggeri[5], Enea Poletti[5], Pedro Guimarães[5], Neil S. Lagali[6]. [1]Department of Ophthalmology, Innlandet Hospital Trust, Elverum, Norway; [2]The Norwegian Dry Eye Clinic, Oslo, Norway; [3]Unit of Regenerative medicine, Department of Medical Biochemistry, Oslo University Hospital, Oslo, Norway; [4]Institute for Applied Computer Science/Automation, Karlsruhe Institute of Technology, Karlsruhe, Germany; [5]Department of Information Engineering, University of Padova, Padova, Italy; [6]Department of Ophthalmology, Faculty of Health Sciences, Linköping University, Linköping, Sweden.

Purpose: To quantify corneal sub-basal nerve and inflammatory cell density from large-area corneal mosaics in order to evaluate the possible differences between right and left eye and to compare the results of manual versus automated analysis.

Methods: Using laser-scanning in vivo confocal microscopy, the central cornea of 83 subjects (166 eyes) was imaged by an experienced examiner. Images of the sub-basal plexus were used to assemble the best possible mosaic. Mosaics from both eyes of each patient were thereafter subjected to both manual and automated tracing of nerves and manual counting of inflammatory cells. ImageJ/ NeuronJ was used for manual analysis while a custom program was used for automated analysis. The results of both manual and automated density analysis were compared.

Results: Large-area mosaics could be assembled in all eyes, with an average mosaic size of 6.3 mm^2, representing an average of 40 single confocal fields of view. A single mosaic took an average of 106 minutes to assemble from an average of 522 individual input image frames by a fully automated procedure. Mosaic tracing by the manual Neuron-J method took on average 35 minutes per mosaic, and yielded sub-basal nerve density values that differed from the fully automated method, which took less than one minute per mosaic to fully trace and analyze. Left and right eyes were often found to have differing nerve patterns and nerve and cell densities, while the mosaics also revealed local variations in nerve and inflammatory cell density.

Conclusions: High quality, large-area mosaics of the corneal sub-basal nerve plexus can be obtained and assembled with an automated approach. Nerve and cell density, however, can vary with eye, analysis method, and microscopic region within the plexus. This brings into question the validity of multiple single-image and single-eye analyses of these parameters.

Commercial Relationships: Reza A Badian, None; **Tor P. Utheim**, None; **Stephan Allgeier**, None; **Bernd köhler**, None; **Alfredo Ruggeri**, None; **Enea Poletti**, None; **Pedro Guimarães**, None; **Neil S. Lagali**, None

Program Number: 1638 **Poster Board Number:** D0146
Presentation Time: 8:30 AM–10:15 AM
Characterization of corneal epithelia in Sjögren's syndrome associated dry eye disease by In Vivo Confocal Microscopy
Anne S. Irvine[2, 1], Christopher J. Irvine[2, 1], Tudor Tepelus[1], Gloria Chiu[3], Srinivas R. Sadda[1, 4], Olivia L. Lee[1, 4]. [1]DIRC, Doheny Eye Institute, Los Angeles, CA; [2]School of Medicine, Universidad Autonoma de Guadalajara, Guadalajara, Mexico; [3]Ophthalmology, USC Eye Institute, Keck School of Medicine, Los Angeles, CA; [4]Ophthalmology, David Geffen School of Medicine, University of California Los Angeles, Los Angeles, CA.
Purpose: To describe the morphological features of the corneal epithelial layers in patients with dry eyes associated with Sjögren's syndrome (SS) by using in vivo confocal microscopy (IVCM).
Methods: Central cornea images were prospectively captured from 43 eyes with clinically diagnosed Sjögren's syndrome and 10 age matched healthy control eyes using In Vivo Laser Scanning Confocal Microscopy (Heidelberg Retina Tomograph Rostock Cornea Module - HRT III RCM). Morphological changes of the corneal superficial, wing, and basal epithelial layers were evaluated and the quantification of wing and basal cells density was performed by two independent masked observers, using the semi-automated cell count software provided by the microscope.
Results: Images obtained by IVCM from 53 eyes were analyzed. As compared to controls, SS affected eyes exhibit increased desquamation, larger cells and enhanced reflectivity of the superficial epithelial cells. Local alterations were observed within the wing and basal epithelial layers, including enlarged and irregularly shaped cells. The density of the wing cells was similar between the SS group and the control group (4923±838 cells/mm2 vs. 4762±416 cells/mm2, p=0.56), while the density of basal epithelial cells showed a tendency of reduction in the affected eyes, without reaching statistical significant difference between the SS group and the control group (5628±581 cells/mm2 vs. 6076±459 cells/mm2, p=0.05).
Conclusions: IVCM reveals morphological changes in the corneal epithelial layers of patients with SS as compared to normal corneas. Yet, the overall density of wing and basal cells for our cohort is similar between the control and diseased corneas. IVCM may be a useful tool that allows detection of subclinical changes in the corneal epithelium of eyes affected by SS.
Commercial Relationships: Anne S. Irvine, None; **Christopher J. Irvine**, None; **Tudor Tepelus**, None; **Gloria Chiu**, Allergan (C), Allergan (F); **Srinivas R. Sadda**, Allergan (F), Carl Zeiss Meditec (C), Carl Zeiss Meditec (F), Carl Zeiss Meditec (F), Genentech (C), Genentech (C), Genentech (F), Optos (F), Regeneron (C); **Olivia L. Lee**, Allergan (C), Allergan (F)

Program Number: 1639 **Poster Board Number:** D0147
Presentation Time: 8:30 AM–10:15 AM
Vascular and morphologic analysis of pterygia evaluated by in vivo confocal microscopy
Olivia L. Lee[1, 2], Ping Huang[1], Tudor Tepelus[1], Jianyan Huang[1], Vikas Chopra[1, 2], Srinivas R. Sadda[1, 2]. [1]Doheny Image Reading Center, Doheny Eye Institute, Los Angeles, CA; [2]Department of Ophthalmology, David Geffen School of Medicine, University of California Los Angeles, Los Angeles, CA.
Purpose: To evaluate the vascular and morphological characteristics of the cornea and conjunctiva in patients with unilateral primary pterygia by comparison with the fellow eye.
Methods: Six patients with unilateral primary pterygia were recruited for this prospective study. In the study eye, the body of the pterygium and clear central cornea were imaged using *In Vivo* Laser Scanning Confocal Microscopy (Heidelberg HRT III RCM). In the fellow

eye, the corresponding nasal bulbar conjunctiva and central cornea were imaged to provide controls for comparison. The presence of inflammatory cells and blood vessels in the pterygium were evaluated by examination of three 400 x 400 micron fields per eye. The density of basal corneal epithelial cells, keratocytes, and dendritic cells were also analyzed and compared between eyes using the semi-automated cell analysis software provided by Heidelberg.
Results: The stroma of pterygia demonstrated evidence of densely packed hyperreflective tissue in parallel arrangement with linearly-oriented blood vessels. The mean number of vessels within pterygia was 35.6±4.4/mm^2 compared to 13.8±4.2/mm^2 in normal nasal conjunctival of the fellow eyes (p<0.01). The mean dendritic cell density in the pterygia was significantly higher than in the nasal bulbar conjunctiva of the fellow eyes (106.9±36.5/mm^2 vs 23.1±15.6/mm^2, P < 0.001). The mean density of basal epithelial cells in the central cornea in the pterygia eyes and control eyes was 5172.0±466.1 cells/mm^2 and 6333.3±446.7 cells/mm^2 respectively (p<0.05). The density of dendritic cells in the clear central cornea was 44.4±11.9/mm^2 in pterygia eyes, which was significantly higher than in the fellow eyes (6.9±5.8/mm^2, P < 0.05). There was no significant difference in the density of keratocytes in the anterior and posterior stroma between the two groups (p>0.05).
Conclusions: In vivo confocal microscopy may be helpful in evaluating morphologic and vascular alterations of pterygia. Our study demonstrates increased corneal and conjunctival dendritic cell density and decreased corneal epithelial cell density in eyes with pterygia. These findings suggest the potential for use of *In vivo* confocal microscopy in the evaluation and monitoring of patients with pterygia.
Commercial Relationships: Olivia L. Lee, Allergan (C), Allergan (F); **Ping Huang**, None; **Tudor Tepelus**, None; **Jianyan Huang**, None; **Vikas Chopra**, None; **Srinivas R. Sadda**, Allergan (C), Allergan (F), Allergan (R), Carl Zeiss Meditec (C), Carl Zeiss Meditec (F), Carl Zeiss Meditec (R), Optos (C), Optos (F), Optos (R)

Program Number: 1640 **Poster Board Number:** D0148
Presentation Time: 8:30 AM–10:15 AM
Automated, software-based objective assessment of Fuchs Corneal Dystrophy severity utilizing retroillumination photography analysis
Allen O. Eghrari, Brian Garrett, Aisha Mumtaz, Elyse J. McGlumphy, Benjamin W. Iliff, Armand Edalati, S. Amer Riazuddin, John D. Gottsch. Wilmer Eye Institute, Johns Hopkins Hospital, Baltimore, MD.
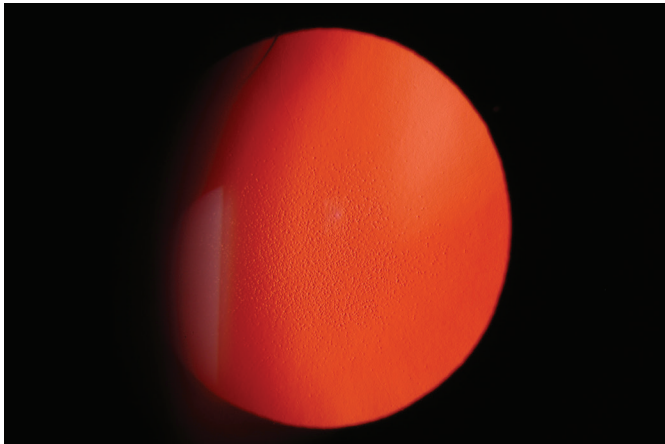**Purpose:** Retroillumination photography analysis (RPA) is an objective tool for assessment of the number and distribution of guttae in eyes affected with Fuchs Corneal Dystrophy (FCD). RPA provides a distinct baseline of 0 guttae, in contrast to variable baseline measurements of pachymetry, and can provide high resolution of disease progression. Current protocols include manual processing of images; here we demonstrate a software-based system for automated analysis across various levels of FCD severity.
Methods: Retroillumination photographs of ten FCD-affected corneas across various levels of severity were acquired and total counts of guttae summated manually using methods we have previously described. For each cornea, a single image was then loaded into ImageJ software. Processing included reducing color variability and subtracting background noise. Reflection of light from each gutta was identified as a local area of maximum intensity and counted automatically. Background irregularities due to lenticular or tear film abnormalities specific to each individual were adjusted by titrating noise tolerance levels to each cornea. Quality control was

conducted by examining a small region of each image with automated overlay to ensure appropriate coverage of individual guttae.

Results: A total of ten retroillumination photographs were analyzed. The Krachmer score, a 1-to-5 grading scale assigned clinically through slit-lamp biomicroscopy, ranged from a severity level of 2 to 5 in the set of analyzed corneas, consistent with mild to severe disease. Automated counts demonstrated a strong linear correlation with manual counts in the set of images (R^2=0.93), each of which ranged from 189 to 9211 guttae.

Conclusions: Software-based, automated RPA allows for rapid grading of FCD severity with high resolution across mild, moderate, and advanced levels of disease severity. This technique may prove beneficial for clinical trials which require precise characterization of disease severity using efficient methods.

Retroillumination photograph of a cornea affected by Fuchs Corneal Dystrophy. Guttae, excrescences of Descemet membrane, are appreciated centrally.

Commercial Relationships: Allen O. Eghrari, None; **Brian Garrett**, None; **Aisha Mumtaz**, None; **Elyse J. McGlumphy**, None; **Benjamin W. Iliff**, None; **Armand Edalati**, None; **S. Amer Riazuddin**, None; **John D. Gottsch**, None
Support: NIH Grant K12 EY015025

Program Number: 1641 **Poster Board Number:** D0149
Presentation Time: 8:30 AM–10:15 AM
Automated detection of Fuchs' dystrophy through a machine learning algorithm using Pentacam data
Irene Ruiz Hidalgo[1, 2], Pablo Rodriguez Perez[3], Jos J. Rozema[1, 2], Carina Koppen[1, 2], Sorcha S. Ni Dhubhghaill[1], Nadia Zakaria[1, 2], Marie-Jose B. Tassignon[1, 2]. [1]Ophthalmology, Antwerp University Hospital, Edegem, Belgium; [2]Medicine and Health Sciences, University of Antwerp, Antwerp, Belgium; [3]ICMA, Consejo Superior de Investigaciones Científicas, Zaragoza, Spain.

Purpose: Fuchs' dystrophy is a bilateral, age-related pathology of the corneal endothelium causing clinical symptoms, such as loss of visual acuity, guttae formation and increased central corneal thickness. Diagnosis is typically performed by slit lamp and specular microscopy evaluation, which is at times challenging in performance and interpretation. In this work we present the first results of a machine learning algorithm using only Pentacam topography/tomography data that may eventually assist physicians in the screening of Fuchs' dystrophy.

Methods:
This retrospective study includes data of 296 eyes, divided into two groups: 138 eyes diagnosed with Fuchs' dystrophy (57.25% females and 42.75% males, mean age = 74.6 years, range 53 - 92 years), and

158 normal control eyes (63.29% females and 36.71% males, mean age = 63.3 years, range 50 - 91). Exclusion criteria were having a spherical equivalent refraction above 10 D, recent wear of hard contact lenses and previous corneal surgery. From the Pentacam we extracted 244 variables regarding densitometry, pachymetry and corneal volume, which were introduced into Weka, a computer program that supports data mining tasks. A support vector machine (SVM) algorithm was then run to obtain an automated binary classification of these eyes.

Results: Precision, confusion matrix and area under the curve (AUC) were calculated for both groups and are shown in the table, along with the accuracy estimated through a 10-fold cross-validation (CV).

Conclusions: Pentacam data alone can provide a fairly good detection of Fuchs' dystrophy and may therefore be useful alongside specular microscopy. Corneal densitometry parameters were found to be the most discriminant features, thus making these parameters good predictors of Fuchs' dystrophy. In a later stage of the study subjects showing early signs of the disease could be included to assess the suitability of this automatic classification for early diagnosis.

Actual class \ Predicted class	Fuchs'	Normal	10-fold CV accuracy	Precision	Sensitivity	AUC
Fuchs'	105	27	85.52%	0.875	0.795	0.934
Normal	15	143		0.841	0.905	0.926

Results table

Commercial Relationships: Irene Ruiz Hidalgo, None; **Pablo Rodriguez Perez**, None; **Jos J. Rozema**, None; **Carina Koppen**, None; **Sorcha S. Ni Dhubhghaill**, None; **Nadia Zakaria**, None; **Marie-Jose B. Tassignon**, None

Program Number: 1642 **Poster Board Number:** D0150
Presentation Time: 8:30 AM–10:15 AM
Multimodal and multiplex spectral imaging of rat cornea ex vivo using a white-light laser source
Nozomi Hagiwara[1], Yuichi Kaji[1], Hideaki Kano[2], Hiroki Segawa[3], Tetsuro Oshika[1]. [1]Department of Opthalmology, University of Tsukuba, Tsukuba, Japan; [2]Institute of Applied Physics, University of Tsukuba, Tsukuba, Japan; [3]Department of Chemistry, School of Science, The Uninersity of Tokyo, Bunkyo, Japan.

Purpose: Raman scatting, which is the inelastic scatting of a photon, has molecular-specific wavelength distribution. The analysis using coherent Raman scatting can visualize molecular structural information in vivo without pretreatments, tissue preparations and staining.

In this study, we developed a new coherent Raman microscope using white-light laser source and try to observe various molecular localization of rat cornea ex vivo.

Methods: The cw Q-switched microchip Nd : YAG laser is used as the light source.

The output beam (1064 nm) is divided into two. The one is used directly as the pump radiation, and the other is used as seed laser pulses which are introduced into a photonic crystal laser (PCF) to generate supercontinuum (SC : white-light laser) for Stokes radiation. We irradiate these two kinds of laser light to rat cornea, soaked normal saline, and analyzed the transmitted coherent anti-Stokes Raman scatting (CARS), signals by mycrospectroscopy.

Results: Analyzing CARS spectrum, we obtained stereoscopic information about molecular localization of purine ring, phenylalanine moiety, CH_2 stretch. It means that we can get 3D image about localization of nucleic acid, protein, and lipid in cornea.

Conclusions: We succeeded in development the multimodal nonlinear spectral imaging microscope which can visualize localization of nucleic acid, protein, and lipid in cornea. Using this technology, detailed molecular structural information will be observed with slit-lamp microscope near future.

Program Number: 1643 **Poster Board Number:** D0151
Presentation Time: 8:30 AM–10:15 AM
Lipid Hydrocarbon Chain Conformation of Surface Lipid Films by Raman Spectroscopy and the Rate of Evaporation

Douglas Borchman, Samihay Sledge, Heidi Michiel, Emily Dennis, Dylan Gerlach, Rahul Bhola. Ophthalmology and Visual Sciences, University of Louisville, Louisville, KY.

Purpose: Meibum hydrocarbon chain conformation changes with dry eye and may be important for function. The conformation of meibum on the surface of tears is unknown. Others have shown that surface films composed of meibum do not inhibit the rate of evaporation in *vitro*. We tested the idea that components in human tears such as proteins interact with human meibum placed on the surface of human reflex tears and together they inhibit the rate of evaporation. Much of what we know about the evaporation through lipid films comes from studies focused on retarding the evaporation from large reservoirs. We repeated conflicting earlier studies relevant to reservoirs involving the inhibition of evaporation by lipids.

Methods: Raman spectroscopy (of 5 mm^2 areas) was used to measure the hydrocarbon chain conformation of human meibum and lipid alcohols containing 12 to 26 carbons on the surface of human reflex tears in *vitro* and to confirm the formation of a continuous film. A range of lipid thicknesses up to a very thick layer of lipids relative to physiological thicknesses were studied. Evaporation rates were measured gravimetrically.

Results: Both lipids naturally present in tears and added meibum formed 5 mm^2 "islands" of lipid aggregates on the surface of reflex tears. Raman spectra characteristic of lipid and water were uniform at all regions of the surface, even regions without islands, indicating that a lipid film completely covered the surface. When layered on the aqueous surface, the hydrocarbon chain conformation of meibum and 1-undecanol changed to become dramatically more ordered, containing more *trans* rotamers. A surface film of meibum and a series of lipid alcohols did not inhibit the rate of evaporation significantly.

Conclusions: Meibum is fluid enough to be expressed from the meibomian glands and is likely to become more ordered (viscous) on the surface of the eye. Our previous studies showed that a stiff ordered molecular arrangement results in a more elastic lipid layer in which molecules are able to rearrange during compression and expansion. Our results concur with studies suggesting that it is questionable whether lipid layers significantly inhibit the rate of evaporation on the surface of the eye or on the surface of reservoirs.

Program Number: 1644 **Poster Board Number:** D0152
Presentation Time: 8:30 AM–10:15 AM
Direct measurement of corneal tissue water content by reflection imaging at Terahertz Frequencies

Shijun Sung[1, 2], Somporn Chantra[3], Neha Bajwa[2], Ryan Mccurdy[2], Gintare Kerezyte[2], James Garritano[2], Jean-Pierre Hubschman[3], Warren Grundfest[2], Sophie X. Deng[3], Zachary Taylor[2]. [1]Electrical Engineering, University of California, Los Angeles, Elk Grove, CA; [2]Center for Advanced Surgical and Interventional Technology, UCLA, Los Angeles, CA; [3]Jules Stein Eye Institute, Los Angeles, CA.

Purpose: Many pathologies such as Fuchs' endothelial Dystrophy and pseudophakic bullous keratopathy result in increased corneal tissue water content (CTWC). However, accurate, non-invasive, *in vivo* measurement of CTWC remains elusive. This study reports direct, non-contact measurement of CTWC in rabbit models using a novel reflectomertry technique based on Terahertz (THz) frequency illumination and imaging.

Methods: THz reflectivity images of 12 *in vivo* rabbit cornea were acquired using novel imaging optics. Controls images of healthy cornea were acquired, then CTWC was perturbed through surgical stripping of Descemet's membrane. The resulting increase in corneal issue water was monitored by THz imaging and compared with that computed by CCT measurements acquired with ultrasound pachymetry. THz imagery and pachymetry monitoring were performed over 5 hours following Descemet's membrane stripping. The animals were then euthanized, corneas were resected and sectioned, and the success of membrane stripping verified histologically.

Results: Clear and consistent increases in THz derived CTWC were observed and statistically significant correlations with increasing pachymetry measurements were demonstrated. THz reflection imaging achieved a minimum detectable water concentration difference of < 1.5% using 650 GHz illumination. THz images obtained with ~ 2 mm spatial resolution showed changes in tissue water content distribution throughout the entire extent of the cornea and correlated with the actual water content of the corneas.

Conclusions: THz imaging can provide direct measurement of CTWC in *in-vivo*. The technique is non-contact, sensitive, and does not rely on assumptions of healthy cornea central thicknesses. This allows the technology to be robust to physiologic variation and feasible to be translated into clinical application.
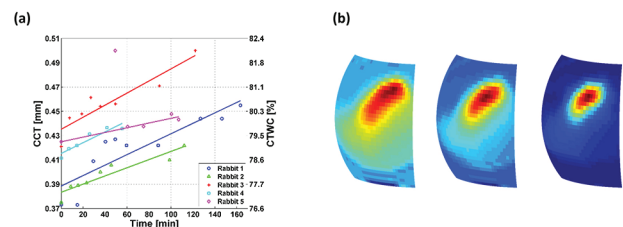

Figure 1: (a) Central cornea thickness (CCT) and computed corneal tissue water content as a function of time following corneal tissue water content perturbation procedure. **(b)** Images (650 GHz illumination) of cornea eye displaying reflectivity decrease from correlated with drop in corneal water content.

Program Number: 1645 **Poster Board Number:** D0153
Presentation Time: 8:30 AM–10:15 AM
Mouse Genomic Loci Modulating Corneal Thickness

Rebecca King[1], Michael A. Hauser[2], Louis R. Pasquale[3], Janey L. Wiggs[4], Allison E. Ashley-Koch[5], R Rand Allingham[6], Eldon E. Geisert[1]. [1]Ophthalmology, Emory School of Medicine, Atlanta, GA; [2]Medicine and Opthalmology, Duke University, Durham, NC; [3]Glaucoma Service, Massachusetts Eye and Ear Infirmary, Boston, MA; [4]Ophthalmology, Harvard Medical School, Boston, MA; [5]Medicine, Duke University, Durham, NC; [6]Opthalmology, Duke Univeristy, Durham, NC.

Purpose: Central corneal thickness (CCT) is a highly heritable ocular trait that impacts several human disorders including primary open angle glaucoma (POAG).
Methods: We have used a mouse genetic reference panel (the BXD RI strain set) to define mammalian genomic loci modulating CCT with a total of 378 mice from 67 BXD RI strains (between 60-100 days of age). The mice were deeply anesthetized and the eyes were positioned in front of the lens of the Phoenix Micron IV Image-Guided OCT system or the Bioptigen OCT system. CCT data for each strain was averaged and used to identify quantitative trait loci (QTLs) modulating this phenotype using the bioinformatics tools on GeneNetwork (www.genenetwork.org).
Results: This analysis reveals one significant QTL on Chr 13 and several suggestive QTLs on Chr 6, Chr 16 and Chr 19. The significant locus on Chr 13 10 to 20 Mb was examined further to define potential candidate genes modulating this eye phenotype. The 13 Mb region under the mouse Chr 13 peak distributes over 4 chromosomes in the human: Chr 1, Chr 6, Chr 7 and Chr 10. Using the eye and retina microarray datasets (HEIMED and HEI Retina) on GeneNetwork, we identified 11 genes with cis-QTLs that could be modulating CCT in the BXD RI strain set. In addition there were 28 genes with nonsynonymous SNPs. Together this represented 38 candidate genes on Chr 13 between 9 and 22 Mb. These candidate genes were examined to determine if they are potential risk factors for human glaucoma using meta-data from the NEIGHBOR-GLAUGEN GWAS. Several SNPs located in an intragenic region near *ELMO1* demonstrated nominal significance ($p = 0.001$ for lead SNP rs9986865).
Conclusions: This approach can identify candidate genes modulating CCT in the mouse and a potential risk factor for primary open angle glaucoma. We are in the process of defining genes in this mouse locus that are associated with the regulation of CCT in humans.